The Effect of In Vitro Gastrointestinal Condition on Aggregation of Nano Silica Particles

Degree Project in Food Technology

LUNDS UNIVERSITET

Lunds Tekniska Högskola

Shuai Bai

Department of Food Technology, Faculty of Engineering (LTH), Lund University Lund,

September 2018

Abstract

The presence of Nano particles in food is a topic that have gain much attention lately. The aim of this study is to investigate the aggregation behavior of nano silica under in vitro gastrointestinal conditions using asymmetric flow field flow fractionation (AF4) coupled with several detectors. Major part of this work is to find a suitable condition for the experiments. With measurements of Z-potential and utilizing the DLVO theory a suitable condition for the experiment is developed. To avoid membrane interaction a relatively high surface energy membrane (Regenerated cellulose) is most suitable. The carrier liquid should have a low ionic strength and a pH away from the iso electric point to contribute to a greater electrostatic repulsion. These actions lead to less membrane interaction as well as ensuring the carrier liquid does not interfere with the aggregation.

Parameters in the gastrointestinal environment like the ionic strength, pH, presence of proteins and Bile salts are altered individually during experiments, to examine the effect of each parameter. Under gastric conditions the high ionic strength and low pH gives the silica particles a poor electrostatic repulsion causing the particles to aggregate. The enzymes present in the gastric conditions is insufficient to cover the particles and might causes bridging. The ionic strength and pH conditions of the intestinal fluids cause a small electrostatic repulsion but not enough to entirely prevent aggregation, instead the large number of mixed enzymes will initiate aggregation by protein-protein interaction. The aggregation of silica particles is greatly reduced when bile salt is introduced to the fluid. Bile salt will act as a surfactant stabilizing the suspension.

Keywords: Silica nanoparticles, in vitro digestion, Aggregation, Asymmetrical flow field flow fractionation, DLVO, membrane interaction.

Abbreviations

AF4	Asymmetrical flow field flow fractionation
dRI	differential Refractive Index
MALS	Multi Angle Light Scattering¨
MQ	Milli. Q
SGF	Simulated Gastric Fluid (only ions)
SGF_pH	Simulated Gastric Fluid pH corrected (pH3)
SGF_pH_Enzyme	Simulated Gastric Fluid pH corrected with enzymes
SIF	Simulated Intestinal Fluid (only ions)
SIF_pH	Simulated Intestinal Fluid pH corrected (pH7)
SIF_pH_Enzyme	Simulated Intestinal Fluid pH corrected with enzymes
RC	Regenerated Cellulose
PES	Poly Ether Sulfone
PF	Poly Fluorinated polymer
r_{hyd}	Hydrodynamic radius
r_{rms}	Root Mean Square radius
EDL	Electric Double Layer

Table of content

1. Introduction

Silicon dioxide (silica) is widely used as additives in food, for example as anti-caking agent. Although usually stated on the package label, the size distribution and morphology of the particles is usually unknown. The size distribution of particles is of big importance as this can indicate the presence of nanoparticles. Nano particles have different properties to larger particles and existing knowledge of the substance is not always applicable to nanoparticles. The effects of nanoparticles on human health is rather unexplored. But recent studies have shown that nanoparticles from silica have cytotoxic effect on human cells[1]. This has led to an increasing debate regarding health and safety surrounding the use of nanosized ingredients. Therefore, the size distribution, and aggregation properties are important factors to investigate for the safety assessment of these particles. The challenge is to find a suitable method to examine the size and aggregation without the method interfering with the process. The aim of this degree project is to determine how the flocculation of silicon dioxide is affected by the environments in the digestive system using a static in vitro method. How changes in the environment such as pH, ionic strength and surface-active molecules may affect flocculation and, thus change the size distribution. Is it possible to have freely dispersed nanoparticles inside the digestive system?

Asymmetric flow-field-flow-fractionation (AF4) coupled with multiangle light scattering (MALS) and differential refractive index (dRI) detection is a powerful separation technique used to detect the size distribution of particles and macromolecules. AF4 is particularly suitable for this project as the conditions during separation are easily modified to suite the purpose, and the lack of stationary phase ensures a low shear force that minimizes disruption of aggregates[2].

2. Theory

2.1. Flow field-flow fractionation (flow FFF, AF4)

Flow FFF is a family of separation methods utilizing the differences in diffusion rate of particles and macromolecules. The development can be traced back to the late J. Calvin Giddings and his group in late 1970. Different development steps have led to the asymmetric flow FFF (AF4), which is the most utilized method and is the design used in all commercial instruments [3] including the setup used during this thesis.

2.1.1. Basics

The separation of macromolecules and particles takes place in a thin trapezoidal channel without any stationary phase, instead the separation happens at an accumulation wall constituted by an ultra-filtration membrane. The carrier is pumped through the channel creating a laminar flow, this flow is called the carrier flow or detector flow. The carrier also passes through the membrane creating a flow perpendicular to the detector flow referred to as the cross-flow. Samples introduced into the channel are transported along the channel by the carrier flow and the cross flow pushes the sample towards the accumulation wall. As the sample cannot pass the membrane the sample is concentrated at the accumulation wall creating a thin layer of sample [4]. In brief AF4 have two different elution modes, the steric/hyper layer mode for particles larger than 1µm and the Brownian mode also called the normal elution order mode for all particles under 1µm [5]. Experiments conducted in this thesis is focused on Brownian mode.

Because of the Brownian motion components yield a transport away from the accumulation wall, while the cross flow pushes the components towards the membrane. Sample components will establish an equilibrium, a steady state concentration distribution where the drift from cross flow is in balance with the diffusion rate. As particles with small size have higher diffusion rate, small particles will on average migrate further away from the accumulation wall than larger particles. Since the carrier flow flows through a very narrow channel with low flow rate the flow is laminar. Particles farther away from the wall is caught in the flow stream with a higher carrier flow velocity and is therefore transported faster through the channel [4]. The principal of AF4 separation is illustrated in Fig. 1

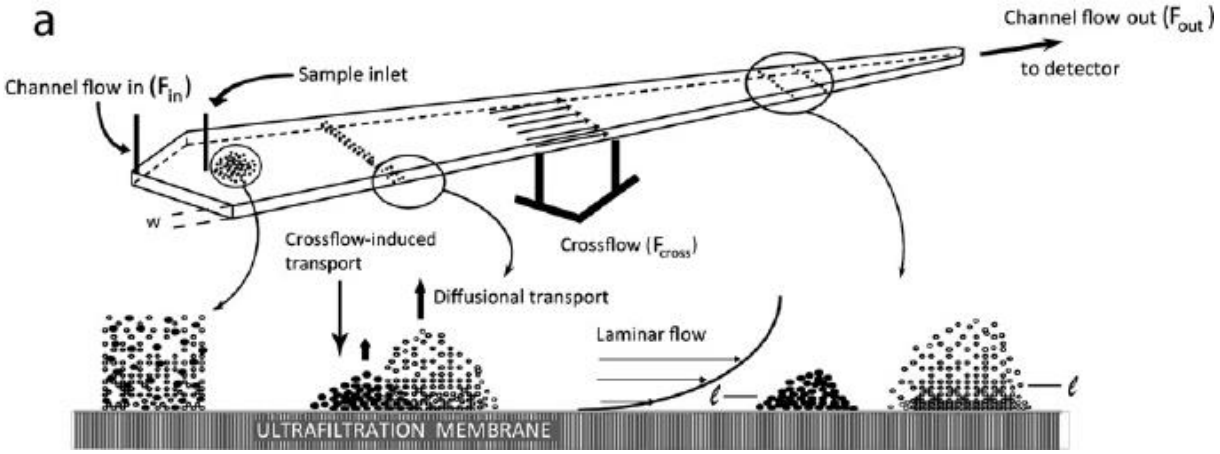

Fig. 1. Illustration of separation in AF4. Particles of different size is loaded as a homogeneous mixture into the channel. The sample is focused and relaxed, when the elution flow starts different components will migrate with different velocities.[6]

The diffusion coefficient D can be calculated using Eq.1 [5].

$$D = \left(\frac{t^0 Q_c w^2}{6V^0}\right) * \frac{1}{t_r} \qquad \text{Eq.1}$$

Where t^0 is the void time, Q_c the cross flow, w the channel thickness, V^0 is the geometric volume of the channel and t_r is the retention time of that specific component.

The size of the particles and macromolecules based on its diffusion rates is indicated by its hydrodynamic radius r_{hyd} also known as Stokes radius, this can be calculated with the Stokes-Einstein equation (Eq.2)

$$r_{hyd} = \frac{kT}{6\pi\eta D} \qquad \text{Eq.2}$$

Where k is the Boltzmann constant, T is the absolute temperature, η is the dynamic viscosity of the solvent. When combining Eq1 and Eq2 the r_{hyd} can be directly calculated from the retention time from AF4 Eq. 3[5].

$$r_{hyd} = \frac{kTV^0}{6\pi\eta Q_c w^2} * t_r \qquad \text{Eq.3}$$

An important parameter to consider when evaluating the separation is the retention parameter RL, as this has a direct effect on efficiency and resolution[3]. The retention parameter for experimental purposes is defined as Eq. 4

$$RL = \frac{t_r}{t^0} \qquad \text{Eq.4}$$

The retention time is obtained directly from the fractogram, whereas the void time should be calculated[3]. For the trapezoidal channel the t^0 can be calculated using Eq.5

$$t^0 = \frac{V^0}{F_{cross}} \ln\left[1 - \frac{w\left(b_0 z' - \frac{b_0 - b_1}{2L} z'^2 - y\right)}{V^0}\right] \qquad \text{Eq.5}$$

To get adequate resolution retention level should be <5.3. This will give a relative error of <5% for the estimation of r_{hyd} [3].

2.1.2. Programed FFF

A problem when analyzing samples with broad size distribution is that small particles need a high cross flow to get an adequate resolution. However, a high crossflow may force the larger particles too close to the accumulation wall which leads to long elution time or in worst case immobilization of the particles[4]. A way to overcome this problem is to use a programed field that start the elution with a high crossflow and over time gradually decreases the cross flow [4]. This way, adequate resolution for the small particle can be obtained, and the larger components can elute under the effect of lower crossflows. A concern arrives from an effect called secondary relaxation effect. As the crossflow decreases the components will need to find a new average distance to relax and if the sample does not have enough time to find it's equilibrium the concentration profile will lag behind leading to components eluting later than predicted [4]. There are different ways to program the decay of cross flow, step-wise, linear, exponential and power programed decay. Exponential decay is the method used in this thesis.

2.1.3. Multi Angle Light Scattering (MALS)

Multiangle light scattering is a powerful method to determine molar mass and root mean square radius (r_{rms}) of macromolecules and particles. This is done without calibration against standards or assumptions regarding particle shape. It is a powerful and popular method to study macromolecules.

Colloids and macromolecules scatters light, the amount of scattered light as a function of the scattering angle θ is described in Eq. 7. It is also clear from this equation that the amount of scattered light depends among other parameters on molar mass of particle.

$$\frac{R_\theta}{Kc} = M_w P(\theta) - 2A_2 M_w^2 P^2(\theta) c + .. \qquad \text{Eq. 7}$$

Where c is the concetration in weight, M_w the weight average molar mass, and A_2 is the second viral coefficient. The excess Rayleigh ratio, R_θ is given by Eq. 8

$$R_\theta = \frac{i_{u,\theta} r^2}{I_0 * (1+\cos^2\theta)} \qquad \text{Eq. 8}$$

Where r is the distance from the scattering particle to the detector,I_0 is the intensity of the incident beam, θ is the angle between incident light to the scattered light and $i_{u,\theta}$ is the intensity of scattered light passing through the detector located at angle θ. The Rayleigh ratio is proportional to the intensity and angle of the scattered light relative to the incident beam. K is an optical constant and is defined as.

$$K = \frac{4\pi^2 n_0^2}{\lambda_0^4 N_A} * \left(\frac{dn}{dc}\right)^2 \qquad \text{Eq. 9}$$

where n_0 is the refractive index of the solvent, λ_0 is the wavelength of the light, N_a is the Avogadro number and $\frac{dn}{dc}$ is the refractive index increment.

The intensity of the scattered light is described by the particle scattering function and is described in Eq.10

$$P(\theta) = \frac{1}{n^2} \sum_{i=1}^{n} \sum_{j=1}^{n} \frac{\sin(u * h_{ij})}{u * h_{ij}} \qquad \text{Eq. 10}$$

where h_{ij} is the distance between i-th and j-th mass element of all mass element in the scattering particle, and λ is the wave length u is described as Eq. 11

$$u = \left(\frac{4\pi}{\lambda}\right) * \sin\left(\frac{\theta}{2}\right) \qquad \text{Eq. 11}$$

Small value of $u * h_{ij}$ indicates a low scattering angle, long wavelength or a small particle, and in this case the $P(\theta)$ can be estimated to Eq.12

$$P(\theta) = 1 - \frac{16n^2}{3\lambda^2} \langle r_{rms,z} \rangle^2 \sin^2\left(\frac{\theta}{2}\right) \qquad \text{Eq.12}$$

Equation 12 is valid for small particles in any shape (or/and low scattering angles) and is the approximation used in this thesis. The diameter of the particle should not exceed half of the wavelength of the incident light λ for the estimation to be valid. For larger particles the more complex Mie theory needs to be used to describe the scattering effects.[4]

The z average r_{rms} is defined as Eq.13 [4].

$$r_{rms,z} = \sqrt{\sum_i n_i * M_i^2 * r_{rms}^2 / \sum_i n_i * M_i^2} \qquad \text{Eq. 13}$$

2.1.4. Size and molar mass determined by light scattering.

In multi angle light scattering the light scattered is measured at several points and from these measurements the intensity at θ =0° is estimated by extrapolation. The reason to estimate the scattering intensity at θ =0° is when combining Eq.13 and Eq.8 the expression simplifies to Eq.14

$$\frac{R_\theta}{Kc} = M - 2A_2M^2c+.. \qquad \text{Eq. 14}$$

And if the second viral coefficient i.e. the interactions between the particles (i.e low sample concentration in the detector) the expression will be simplified to Eq.15

$$\frac{R_\theta}{Kc} = M_w \qquad \text{Eq. 15}$$

So, for low concentration/low second viral coefficient molar mass have a simple relationship with Rayleigh ratio, easily calculated by the estimation of the scattered light at θ =0°.

There are several ways to extrapolate the scattering commonly called the Debye plots. Where R_θ, K, c, is plotted against $\sin^2\left(\frac{\theta}{2}\right)$, the most common methods are Debey, Zimm and Berry. For this thesis, the Zimm method is used, and is described as Eq. 16

$$\frac{Kc}{R_\theta} = \frac{1}{M_w} + \frac{16\pi^2}{3\lambda^2 M_w} * \langle r_{rms,z}\rangle * \sin^2(\frac{\theta}{2}) \qquad \text{Eq.16}$$

From the Debye plots the molar mass can be obtained from the intercept which corresponds to θ =0° and Eq.15. And r_{rms} is determined from the slope. The relationship at the intercept and the slope for the different plots are presented in table. 1.

Table. 1. Different Debye plots and their relationships between intercept and M_w and slope and $r_{rms,z}$.

Plot method	Intercept	Slope
Debey	M	$-\frac{16\pi^2}{3\lambda^2} * \langle r_{rms,z}\rangle$
Zimm	M^{-1}	$\frac{16\pi^2}{3\lambda^2 M_w} * \langle r_{rms,z}\rangle$
Berry	$M^{-1/2}$	$-\frac{8\pi^2}{3\lambda^2 M^{-1/2}} * \langle r_{rms,z}\rangle$

By combining AF4 and MALS, researchers have a powerful tool to investigate macromolecules and particles. The eluted fractions from AF4 provides relatively monodispersed fractions making the evaluation from MALS easier to interpret compared to non-separated samples. Integration of all fractions gives the molar mass distribution. Information regarding shape can be gained from the ratio of r_{rms} and r_{hyd}, this is due to different definitions of the hydrodynamic radius described in Eq. 3 and the root mean square radius described in Eq. 7. The ratios for some idealized shapes have been derived and is given in Table. 2.

Table. 2 . Overview of different r_{rms}/r_{hyd} and corresponding conformation.

r_{rms}/r_{hyd}	Conformation
0.775	Homogeneous sphere
1-1.5	Branched particle
1.5-1.8	Random coil
>2	Elongated, rod like

2.2. Particle interaction

Most of the fundamental theory that is describing colloidal behavior is based dispersions of solid, spherical, homogeneous particle of identical size. This is convenient for this thesis as the samples used in this thesis are monodispersed spherical silica.

2.2.1. The electrical double layer

A particle with a charged surface will affect ions in its vicinity: counterions with opposite charge will attract to the surface while co-ions are repelled. The concentration of counterions near the surface of the particle will be higher than the bulk solution. This uneven distribution of ions near the surface is called the electric double layer EDL. The EDL consist of two layers, the stern layer and the diffuse layer. The Stern layer is in contact with the particle surface and composed of strongly adsorbing ions that are immobile, the diffuse layer consists of mobile ions with a concentration distribution in balance with the kinetic energy and electrical potential energy.

The variation of the electrical potential ψ with distance x is described by Goüy & Chapman and is a simplification that ignores the impact of stern layer. The description is based on the Poisson equation and Boltzmann factor, and therefore called the Poisson- Boltzmann equation Eq. 17.[7]

$$\frac{d^2\psi}{dx^2} = -\left(\frac{e}{\varepsilon_r \varepsilon_0}\right) \sum_i z_i n_{i0} \exp\left(-\frac{z_i e \psi}{kT}\right) \qquad \text{Eq.17}$$

Where ψ is the electrical potential, ε_r is the relative dielectric constant, and $\varepsilon_0$is the permittivity of free space and z_i is the valence number. This is a difficult equation to interpret, but if a few criteria are met the Poisson-Boltzmann equation can be simplified. For a symmetrical binary electrolyte containing large particles ($\kappa r \gg 1$) with low surface potential (<25mV), where κ^{-1} is the Debye length and r the radius of particle. If the criteria are met the Poisson-Boltzmann equation reduces to Eq. 18

$$\psi = \psi_0 \exp(-\kappa r) \qquad \text{Eq.18}$$

This simplification is the Debye -Hückel approximation, the Debye length κ^{-1} is a good measure of the thickness of the electrical double layer. And is described in Eq. 18

$$\kappa^{-1} = \sqrt{\frac{\varepsilon_r \varepsilon_0 k_B T}{2 N_a e^2 I}} \qquad \text{Eq.19}$$

Where I is the ionic strength.

$$I_c = \frac{1}{2} \sum_{i=1}^{n} c_i z_i^2 \qquad \text{Eq.19.1}$$

For full treatise, including derivations of the electric double layer the reader is referred to textbook covering the subject [7]. The Goüy-Chapman theory is invalid close to the charged surface because the Boltzmann assumption does not take the stern layer into account. Stern proposed a more sophisticated model of the electrical double layer taking account an inner stern layer with the thickness of roughly to the radius of the hydrated counterion δ. For Sterns model the Goüy-chapman theory is only valid at x> δ that is outside the immobile layer. The boundary between the immobile phase and the diffusive layer is called the Stern plane the electrical potential ψ decreases linearly from the surface ψ_0 to the Stern plane ψ_δ. In the diffuse layer the potential falls approximately exponentially to zero. The theories and equations expressing the diffusive layer is unaffected by the addition of stern layer, but instead of using the surface electrical potential the stern potential ψ_δ is used instead. A common way to determine the stern potential ψ_δ is to experimentally determine the

electro kinetic potential ξ the Z-potential. This is conducted by measuring the electrophoretic mobility of the particle. The assumption that Z-potential is equal to the stern potential is most valid in a low ionic strength aqueous solution with particles with low surface charge. In electrostatically stabilized lyophobic colloids a layer of water molecules is strongly adsorbed by charge dipole interactions this means that slip plane is inside the diffuse layer. For particles that have adsorbed proteins macromolecules or surfactants the position of the shear plane may move far away from the stern layer measuring a lower Z-potential ξ than the Stern potential so for sterically stabilized systems the assumption that Z-potential is equal to the stern potential is invalid.[7]

2.2.2. Electrostatic repulsion

Charged particles in an aqueous solution will always have an electric double layer, when these double layers start to overlap each other a repulsive force will start to push particles away. This is due to the osmotic pressure created when the excess of counterions in the double layer come in contact with each other. So, the osmotic pressure is higher between particle surfaces and the bulk. Due to the increase in osmotic pressure solvent molecules tend to diffuse to the overlapping region leading to a repulsive effect.

The Poisson Boltzmann equation is used to theoretically describe the repulsion between two interacting double layers. When describing the double layer interaction between two particles it is convenient to consider two separate cases one for large particles with thin double layer ($\kappa r \gg 1$) and one for small particles with thick double layers ($\kappa r \ll 1$). The expressions are described in Eq. 20

$$u_r(h) = \begin{cases} 2\pi\varepsilon_r\varepsilon_0 r\psi_0^2 \ln\left(1 + e^{-\kappa h}\right) & \text{for } (\kappa r \gg 1) \\ \frac{4\pi\varepsilon_r\varepsilon_0 r\psi_0^2 e^{-\kappa h}}{(2+(h/r)} & \text{for } (\kappa r \ll 1) \end{cases} \quad \text{Eq. 20}$$

These equations are valid for surface to surface separation h $u_r(h)$ (repulsion) and is based on monodispersed spherical particles with low surface charge (<25mV)[7]. For this thesis the equation for large particles $(\kappa r \gg 1)$ with thin double layer will be used.

2.2.3. Van der Waals

Except for the repulsive force contributed by the double layer there is an attractive force affecting the particles, the van der Waals (vdW) forces. This attractive force consists of three forces.

- Keesom forces: force between two dipoles
- Debye forces: Force between a dipole and an induced dipole
- London forces: Forces between induced dipoles

London forces contributes most to the vdW forces and relates to the polarizability of the particle, that is the ability to shift the electron density within the particle. The interparticle potential $u_A(h)$ (attractive force) between two isolated particles is given the approximation Eq. 21

$$u_{ij} = \frac{-\Lambda_{ij}}{d_{ij}^6} \quad \text{Eq.21}$$

Where the Λ_{ij} is constant related to molecular polarizabilities and d_{ij}^6 is the distance between two particles center of mass. The total interparticle potential is the sum of all molecular pair interactions. As seen in the approximation the effects of vdW forces is related to the distance to the inverse sixth power, making the force strong only at short distances and weak at long distances.

2.2.4. DLVO

In DLVO theory the electrostatic repulsion $u_r(h)$ is combined with the vdW attractive force to give the total interparticle potential Eq.22.

$$u_{DLVO}(h) = u_r(h) + u_A(h) \qquad \text{Eq.22}$$

Electrostatically stabilized colloids are dependent on the shape of the primary maximum peak as it determines the stability of the colloid. The electrostatic stabilization occurs if the net interaction reaches a maximum energy of more than 25 kT. This is likely to occur in low ionic strength solutions with particles that have sufficient surface charge. Low ionic strength leads to a broader and higher peak as ionic strength affects the Debye length, and the surface potential (estimated by Z-potential) affects the height of the peak.[7]

2.2.5. Steric stabilization.

Most food related colloids contain macromolecules of some kind, polymers proteins or other kind of high molecular weight surface active molecules. These can under the right conditions contribute to steric stabilization. Macromolecules adsorbed at the surface of the particle needs to meet three criteria to achieve an effective steric repulsion: The macromolecules need to cover the entire particle; the layer needs to be sufficiently thick and the macromolecules need to be strongly adsorbed to the surface. When these criteria are met the stability of the colloids are mainly determined by thermodynamic conditions. Segments that is adsorbed to the surface is called train and the segments reaching out towards the solution is called loops, when the segment have two contact points to the surface, and tails when it's at the end of the chain and only have one contact point to the surface. On average, tails extend twice as long from the surface as the loops. When the macromolecules like the solvent, the segments from macromolecules will energetically favor contact with solvent molecules rather than each other. While in a poor solvent segment of the macromolecule will prefer to interact with each other or the surface rather than with solvent, this can lead to chain association and phase separation. The region where the macromolecules is in transition between becoming repulsive polymer chain and attractive chains is called the θ-point. Under θ conditions (θ solvent) the entropy and enthalpy cancels out each other. If the solvent is worse than θ solvent the macromolecules starts to flocculate. The thickness of macromolecules coated on the surfaces is defined as δ, the distance between the surfaces is denoted h. As the surfaces approach each other the segments starts to overlap and in this interpenetrational domain ($\delta \leq h \leq 2\delta$) segment density increases forcing the solvent into the bulk, if it is a good solvent the segment-segment energy will cost more than segment solvent and therefore raise the free energy, leading to repulsion. If the solvent is bad (worse than a θ-solvent) the inter-penetration lowers the free energy causing an attraction.

The mathematical expression for steric stabilization is derived from statistical mechanics and considers two parallel plates, the expression is given by Eq. 23

$$\Delta G_M = (2kTV_p^2/V_s)v^2(\tfrac{1}{2} - \chi)y(h) \qquad \text{Eq.23}$$

Where V_p and V_s are the molar volumes of the polymer/macromolecule and the solvent, V is the number of adsorbed chains per area, $y(h)$ is a function of distance between surfaces dependent on the shape of the segments. χ is the mixing term (Flory-Huggins parameter). If the term $(\tfrac{1}{2} - \chi)$ is positive then the free energy will be positive and lead to repulsion, a negative term leads to an attractive force. When χ=0.5 the term is zero, which means that the solution is a θ solvent. The Flory-

Huggins parameter describes the enthalpic contribution to the free energy using a lattice model. It is defined as Eq.24.

$$\chi = \frac{(2\varepsilon_{12} - \varepsilon_{11} - \varepsilon_{11})z}{2kT} \qquad \text{Eq.24}$$

Where z is the lattice co-ordination number, and $\varepsilon_{12}, \varepsilon_{11}$ and ε_{11} are the contact energy between solvent-segment, segment-segment and solvent-solvent. Another force to consider in steric stabilization is the volume restriction when the two covered surfaces approach each other in the compressional domain $h \leq \delta$. The chains on one surface is compressed by the opposing surface. This is called the elastic repulsion and denoted as ΔG_{VR}, at this proximity to the surfaces vdW attractive force will contribute to an attractive force. This leads to the sum of the steric stabilization to be Eq. 25.

$$u_s(h) = \Delta G_{VR}(h) + \Delta G_m(h) + u_A(h) \qquad \text{Eq.25}$$

If the dispersion is stabilized by macromolecules with charge there is an additional electrostatic contribution. Typical charged macromolecules are proteins and the effect of the electrostatic contribution (repulsion) can be even more important than the steric repulsion, especially when the ionic strength is low. It is very hard to estimate the stabilizing effect of charged macromolecules and the easiest way is to assume that the steric and the electrostatic stabilization acts simultaneously[7].

3. Material and methods

3.1. AF4 and instruments.

The AF4 is from Wyatt technologies with a HPLC pump from Agilent. In all the carrier solvent, 3 mM NaN_3 is added this to prevent bacterial growth in the system [6]. Before the elution, the sample is focused to a narrow band, this is to allow the equilibrium distribution to establish from the accumulation wall (see theory part AF4). The focusing is performed by introducing the carrier flow both from inlet and outlet. The focusing band is a few mm from the sample inlet and is recorded for calculations on r_{Hyd}. The sample load is kept as low as possible to prevent overloading. Overloading may lead to changes in elution time and therefore error in the r_{hyd} calculations[8]. The channel is coupled to MALS and dRI. The MALS detector is normalized with a small isotropic particle with known r_{rms} (Bovine Serum Albumin, BSA). The refractive index increment dn/dc determines both the optical constant and the concentration, both needed to calculate the Molar mass from MALS signal (Eq.14). The calculation is made with estimation that SIF and SGF have the same refractive index as pure water. The calculated value is $v_{SiO_2 \text{ in } H_2O} = 0.0833$ mL/g, calculations in Appendix. 4[9, 10].

3.2. Channel and membrane

The channel used is a short channel provided by Wyatt. The depletion wall is made of a transparent polymetric material, the accumulation wall made of an ultrafiltration membrane supported by a stainless-steel frit. Between the two walls is a spacer with a trapezoidal shape and a thickness of 490µm. To calculate the actual thickness a well-defined molecule is used as reference. For this thesis BSA with a r_{hyd} of 3,4nm is used, the calculations is done with MATLAB fffHydRad 2.1[11]. Regenerated cellulose (RC), poly ether sulfone (PES) and poly fluorinated polymer (PF) are membranes used in this thesis.

3.3. Sample preparation

The colloidal silica from Sigma-Aldrich is stored in a refrigerator at approximately 5℃. The product description is given in Table. 1. The sample is pipetted into the autosampler vial containing the simulated fluids. Different amount of silica is injected to the AF4 to determine the amount of silica needed for sufficient signal as well as preventing overloading. Validation of the performance is done for every new trial using BSA.

Table. 3. Sample properties provided by Sigma-Aldrich.

form	aqueous suspension
concentration	5% (solids)
particle size	0.15 µm
M_w/M_n	0.10
storage temp.	2-8°C

3.4. AF4-method development

Membrane and carrier liquid

The silica particles are analyzed and validated using MQ water. The results are used as a reference point to compare the flocculation behavior. Silica particles are then introduced to the ionic conditions of the digestive system. To ensure the same condition throughout the system, the carrier liquids and the sample liquid are the same. The Ionic strength of the digestive fluids and MQ water is calculated using Eq.18.1, the concentration of ions of the phosphate buffer is first calculated using Henderson Hasselback equation. $\mathrm{pH} = \mathrm{pK_a} + \mathrm{Log}\,\frac{[\mathrm{A}-]}{[\mathrm{AH}]}$ at relevant $\mathrm{pK_a}$. The calculated concentration is used to calculate the ionic strength. Note that all liquids contain $\mathrm{NaN_3}$. The Debye length for a colloidal suspension in an electrolyte solution with monovalent electrolyte is denoted κ^{-1} and described in Eq. 18. The temperature is set on 296K (22.5°C) and gives a relative dielectric constant ε_r of 79(unitless). To find the most suitable membrane RC, PES and PF membrane (all with a molecular weight cut-off of 10kDa) are investigated. The flow setup of each trial including the BSA normalization is presented in Appendix 1, The components in the simulated fluids and phosphate buffer are listed in Appendix.2. The flow scheme and amount injected is illustrated in Appendix 3. Surfactants in the carrier liquid is a common way to analyze nano particles, but utilizing surfactants can greatly affect the aggregates, to avoid interferences surfactants is therefore avoided.

Z-potential

The Z-potential of the particle is measured using the Malvern Zetasizer Nano ZS. Using disposable folded capillary cells DTS1070. The silica is mixed with the different carrier liquids and simulated fluids to 5µg/ml silica. Each sample is measured 3 times with 20 readings each time.

For the surface Z-potential the surface cell is used, a piece of material (membrane) can be glued onto an adapter and immersed into a cuvette containing a solution with tracer particle. The tracer have a known Z-potential, the instruments measures the movement of the tracer particles at different distances from the surface [12]. For each membrane 8 different distances were measured. Each distance is measured 3 times with 20 readings each time.

3.5. AF4-analysis

For the experiments regenerated cellulose membrane is used with a phosphate buffer at pH7 [13] as carrier liquid. Different parameters such as pH and the presence of enzyme and bile salts are now considered. The digestive conditions are kept inside the sample vials. The flow setup of each trial is presented in Appendix 1, the composition of the simulated digestive fluid and phosphate buffer is presented in Appendix 2. The setup and conditions used for each trial is presented in Appendix 3. Both reproducibility and time dependence are evaluated.

4. Results and discussion

4.1. Theoretical and Experimental characterization

4.1.1. Ionic strength/Debye length

The ionic strength in SGF and SIF is higher than in MQ water. The high ionic strength gives a shorter Debye length and allows surfaces to come closer to each other. At a small distance the attractive van der Waals force will start to dominate the electrostatic repulsion, and the surfaces may adsorb to each other.

Table. 4. Ionic strength in different solutions and Debye length of particles in that solution.

	NaN_3 (MQ)	Phosphate Buffer pH 3	Phosphate Buffer pH 7	SGF	SIF	SGF-SIF
Ionic strength	3.1 mM	8 mM	19 mM	81 mM	132 mM	104 mM
Debye length	5.5 nm	3.4 nm	2.66 nm	1.07 nm	0.84 nm	0.9 nm

4.1.2. Amount and Surface area of SiO_2

The amount of SiO_2in the vial is 0.5 µg (0.5 µg/ml) Appendix.3. According to MALS signal based of 5 samples the molar mass of the particle is 1.39*10^9g/mol. The surface coverage is important to predict the interactions between two particles, if the surfaces of the particles are covered with proteins then protein-protein interaction will greatly affect the aggregation. If the surfaces are mostly are uncovered, then bridging might occur. To be able to cover the entire surfaces a concentration of at least $1\ \mathrm{mg/m^2}$ is needed. There are insufficient proteins to cover all surfaces in the gastric conditions, while the high concentration of proteins in the intestinal fluid will covers all particles Table. 5. The calculations for surface area and enzyme coverage of silica particles are presented in Appendix.4.

Table. 5. Amount of protein and coverage of silica particle.

Surface area per silica particle	Volume per silica particle	Total surface area of silica	Enzyme coverage in SGF	Enzyme coverage in SIF
$7.1 * 10^{-14}\mathrm{m^2}$ /Particle	$1.8 * 10^{-23}\mathrm{m^3}$ /Particle	$0.02\ \mathrm{m^2}$	$0.06\ \mathrm{mg/m^2}$	$65.3\mathrm{mg/m^2}$

4.1.3. Results from Z-potential/surface Z-potential.

Membrane Z-potential

The main objective to measure Z-potential is to estimate the electrostatic repulsion coming from the membrane surface. The method is based on placing the membrane between two electrodes inside a solution with tracer particle. Unfortunately, the electrode close distance to each other combined with too high current caused bubbles to form and rise to the membrane covering the membrane with a thin layer of gas making the measurements very unreliable. The results are presented in Appendix. 6.

Particle Z-potential

Particle Z-potential showed a strong correlation to pH, the further away from the isoelectric point (IEP) the stronger the potential, the IEP of silica is around pH4 where the particles have no surface charge[14]. The Z-potential of the silica particle is measured in the different simulated liquids and phosphate buffers. The results are presented in Table.6 and Fig.2.

Table. 6 Measured Z-potential of silica particle in different sample and carrier liquids.

Solution	pH	Ionic strength (mM)	Z-potential (mV)
Phosphate buffer	7	19	-33.6 ± 1.7
Phosphate buffer	3	8	3.9 ± 0.09
SGF	8.8	82	-28.4 ± 1.6
SIF	8.7	132	-27.2 ± 0.8
SGF_pH	2.8	82	2.19 ± 0.5
SIF_pH	8.5	132	-23.1 ± 1.2
SGF_pH_Enzyme	3	82	2.4 ± 0.2
SIF_pH_Enzyme	8.3	132	-20.45 ± 0.3
MQ	10	3	-30.6 ± 1.06

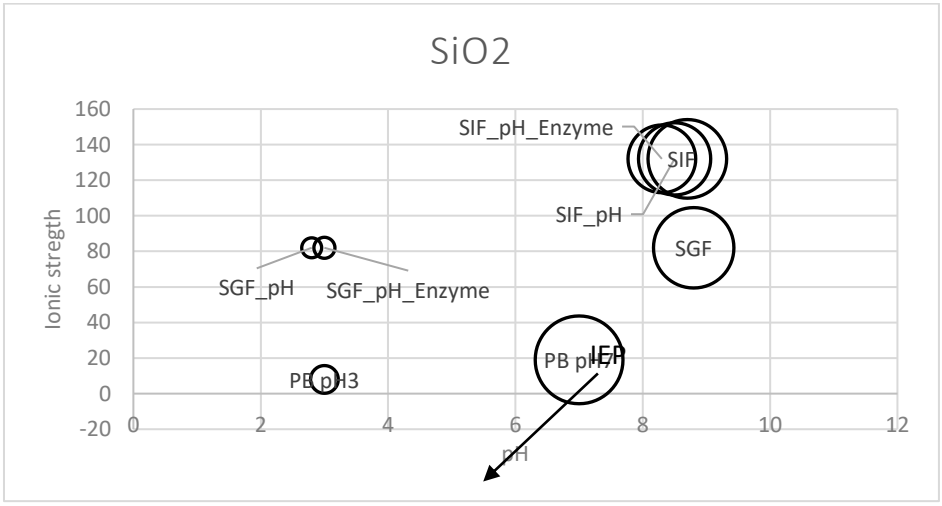

Fig. 2. Illustration of Z-potential of the silica particle in different solutions, the size of the circles represents the value of the Z-potential. The further away from IEP the stronger Z-potential, note that values to the left of IEP are positive.

4.1.4. DLVO

Ionic strength and measured Z-potential is used to calculate the DLVO interaction between particles. The Hamaker constant of amorphous silica in water is set to $0.83 * 10^{20}$J [15], the relative dielectric constant of water is 80(unitless) [16]. Using equation 22 the attractive force and repulsive forces can be calculated and give an insight on aggregation behavior. In Fig. 3 and 4 the repulsive forces are marked as blue line. The attractive force marked as red line. The orange line is the sum of the attractive and repulsive forces. A colloidal system is considered stable if kT is above 25 (J)[7]. Ionic strength, Debye length, pH and Z-potential of particles in the different liquids are presented in Appendix. 7.

Carrier liquid conditions

Silica in MQ water have both a long Debye length and a high Z-potential giving the silica in MQ water a strong electrostatic repulsion making silica in water a stable colloid. The particles in phosphate buffer at pH7 have a shorter Debye length than in MQ-water, but the high Z-potential gives phosphate buffer enough repulsion to prevent aggregation. This makes phosphate buffer at pH7 a suitable carrier liquid as it gives adequate electrostatic repulsion. (Aggregation limited to the sample conditions of digestive fluids) Phosphate buffer at pH 3 have similar Debye length as phosphate buffer at pH7 but the Z-potential is too low to give any repulsive effect. This cannot be used as carrier liquid as the particles will start to aggregate, making it impossible to distinguish if the aggregation is cause by sample condition of carrier condition. Results of DLVO is presented in Fig. 3.

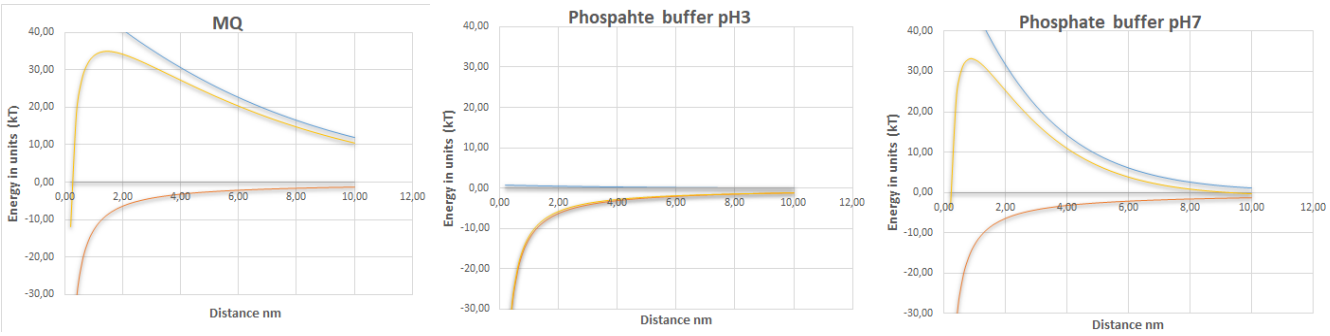

Fig. 3 DLVO for particle in carrier liquid candidates. Blue line represents the electrostatic repulsion the red line is the van der Waals attractive forces. The sum of the attractive and repulsive forces is presented in blue. When the energy barrier is higher than 25 kT it is regarded as stable colloid. Phosphate buffer pH7 have enough electrostatic repulsion to act as suitable carrier liquid.

Sample conditions

The high ionic strength gives a short Debye length for SGF and SIF so even if the Z-potential is high the repulsive force is weaker than MQ-water with similar Z-potential. For SGF_pH the pH is close to the IEP of silica giving a low Z-potential, leading to no repulsion of the particle. Collision will lead to aggregation. The DLVO for particles in different sample conditions is presented in Fig. 4. For solution containing enzymes, the situation becomes more complex, as proteins adsorbs to the particles the interactions between complexes (silica coated with enzymes) can no longer be described only by electrostatic repulsion and attraction, interaction between proteins will greatly affect aggregation[7]. As seen in Table 6. the coverage of protein to silica surface is very different in SGF and SIF, to consider total coverage of the surface the adsorbed amount needs to be at least 1 $\mathrm{mg/m^2}$. For SGF where the particles are not covered bridging can occur, for covered surfaces as in SIF steric

repulsion/attraction are more relevant, see theory section on electrostatic repulsion. To conclude the results from the DLVO calculations, the stability of colloids in different solutions are:

$$SGF > SIF > SIF\_pH > SGF\_pH$$

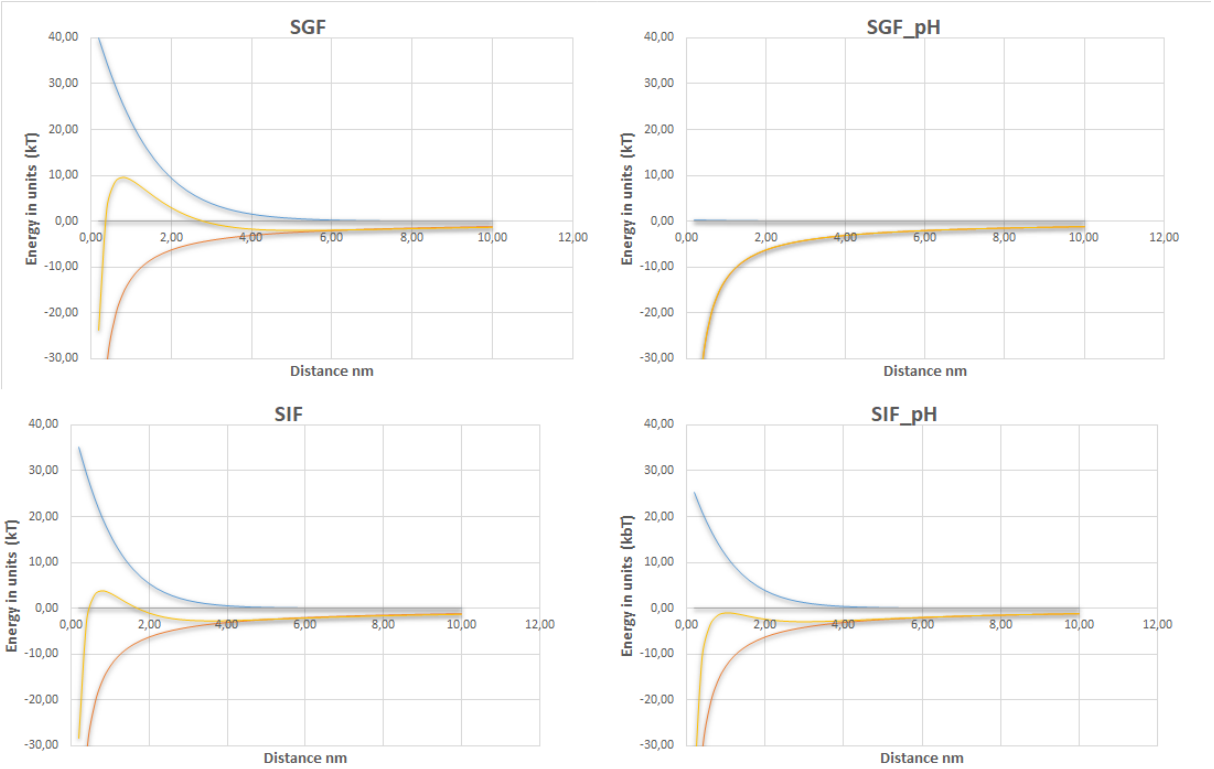

Fig. 4 DLVO for particles in sample conditions. Blue line represents the electrostatic repulsion, red line is the van der Waals attractive forces. The sum of the attractive and repulsive forces is presented in blue. All sample conditions have insufficient repulsion to prevent aggregation. The conditions in SGF_pH lack any repulsion; therefore, attractive force will dominate in short distances.

4.1.5. Contact angle of membranes

The failure to measure the Z-potential of the surface lead to another approach to explain the adsorption to the surface. Contact angle is measured to estimate the surface tension between membrane and water. The surface angle measurements don't reveal any surface energies but gives a good insight on membrane-water interactions. Higher surface angle means a more hydrophobic surface. PES membrane is the most hydrophobic membrane (high surface tension) followed by PF membrane. While the RC membrane is very hydrophilic (low surface tension) and completely wets the surface, as seen in Fig .5. Silica also have a low surface angle and is regarded as hydrophilic [7]. Particles tend to stick to high surface tension surfaces; therefore, RC is the most suitable membrane for further experiments. An important factor that influence the contact angle is how porous the material is, as capillarity also plays a roll. Membrane contact angles cannot be compared with smooth surfaces.

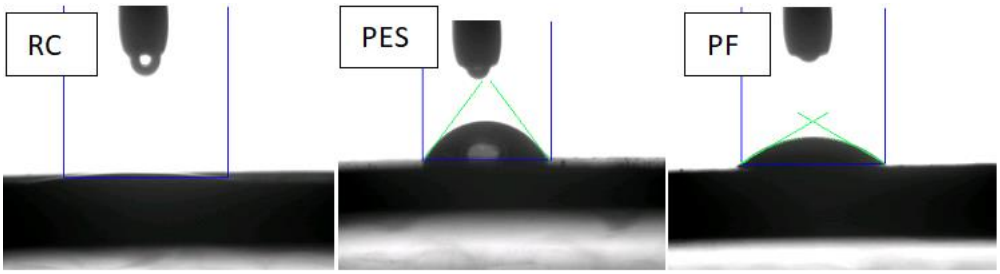

Fig. 5 Contact angle of membranes used during method development. High contact angle with water means a hydrophobic surface and high surface tension. Hydrophilic membranes are preferable as particles tend to stick to high surface tension surfaces. The most suitable membrane for further experiments is RC membrane as it is the most hydrophilic of the candidates. Contact angle of membranes can not be compared with smooth surfaces as capillary influence wetting properties.

4.2. AF4 analysis method development.

4.2.1. Sample parameters

To investigate the sample material and to find a suitable injected amount, silica sample is subjected to MQ water and analyzed using AF4 coupled with MALS detector using RC membrane. Retention levels RL of all experiments are far above 5.3 using Eq. 4 and 5. By injecting 5 sample amounts from 0.015 µg to 0.05 µg the overloading effect is investigated. As seen in Fig. 6 the peaks are symmetrical with no changes in retention time and overloading effect are observed.

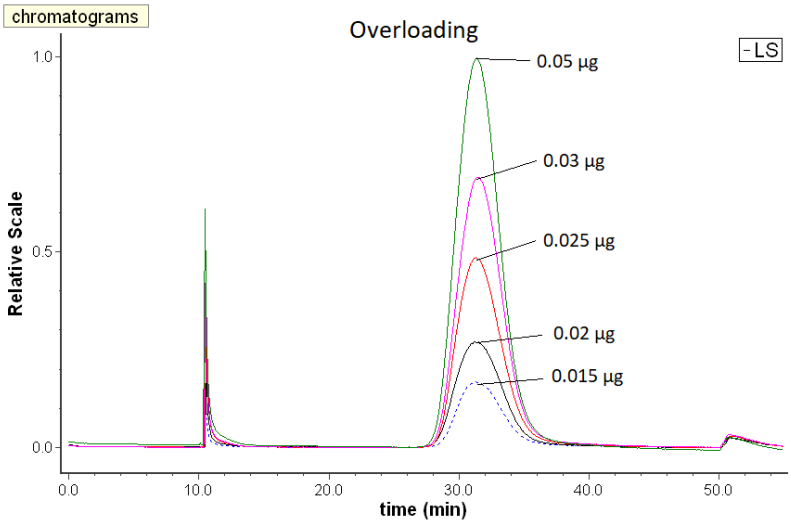

Fig. 6 Overloading effect are investigated to find a suitable injection concentration. MALS signal of 5 different sample concentrations between 1.5 µg/ml to 5 µg/ml shows no change in peak symmetry or retention time. No overloading effect are observed.

The elution profile of three identically prepared samples gives one symmetrical peak with one r_{rms} around 62 nm Fig. 7. This suggest that the silica particles are monodispersed. This result contradicts the stated description of the particle in Table 3. After consulting Sigma-Aldrich, it is confirmed that the size distribution M_w/M_n is in fact 1.0 and not 0.1. Using Eq. 3 the r_{hyd} of the particle is determined to be 72nm. The different radii can now give additional information about the conformation using Table 2, this gives the r_{rms}/r_{hyd} ratio of 0.86 which suggest a shape close to a homogenous sphere. The data is compiled in Table 7. A monodispersed sample makes it easier to interpret the MALS signal, the signal from light scattering are dependent on concentration and size of

particle. The difference in strength of the MALS signal depends solely on the concentration when two samples of monodispersed particles (with same r_{rms}) are compared. This makes it possible to use MALS signal to compare difference in concentration if the particles are the same size.

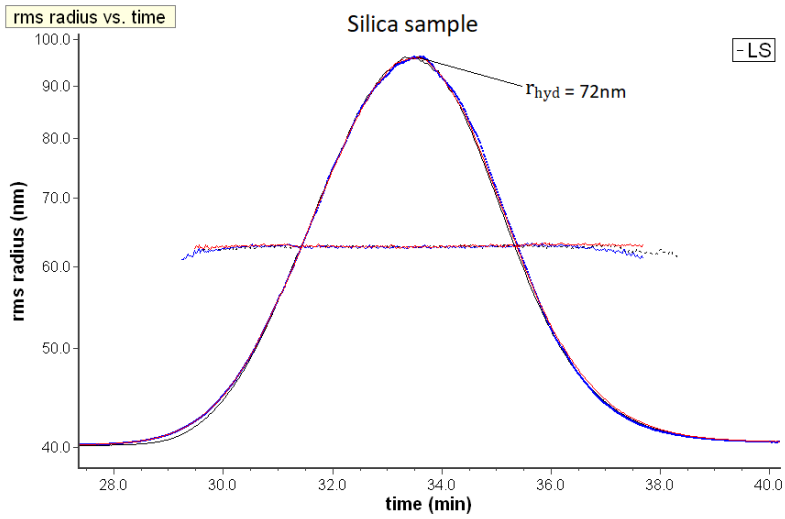

Fig. 7 AF4 analysis of silica sample in MQ water. MALS signal shows one single symmetrical peak with a r_{rms} of 62nm. This indicates a monodispersed sample. The calculated r_{hyd} at the peak maximum at 33.5 min is 72nm.

Table. 7. r_{rms} based on MALS, calculated r_{hyd} and conformation of silica particle.

r_{rms}	r_{hyd}	r_{rms}/r_{hyd}	Shape
62nm	72nm	0.86	Close to homogenous sphere

4.2.2. RC membrane

Silica particles are then subjected to the ionic conditions in the gastric fluid (SGF), both sample and carrier fluid are SGF without pH correction or enzyme added. The samples are analyzed using AF4 with RC membrane coupled with MALS detector. See Appendix.3. The results show obvious changes in peak shape as three identically prepared samples are injected (sequential injection). The peak starts at the same retention time, but the retention time of the peak maximum increases with each sample Fig. 8. The r_{rms} are the same for all three peaks at 63nm, which makes it possible to compare the concentration between the samples. The first sample shows poor recovery, but for each injected sample the recovery increases (Area of peak increases).

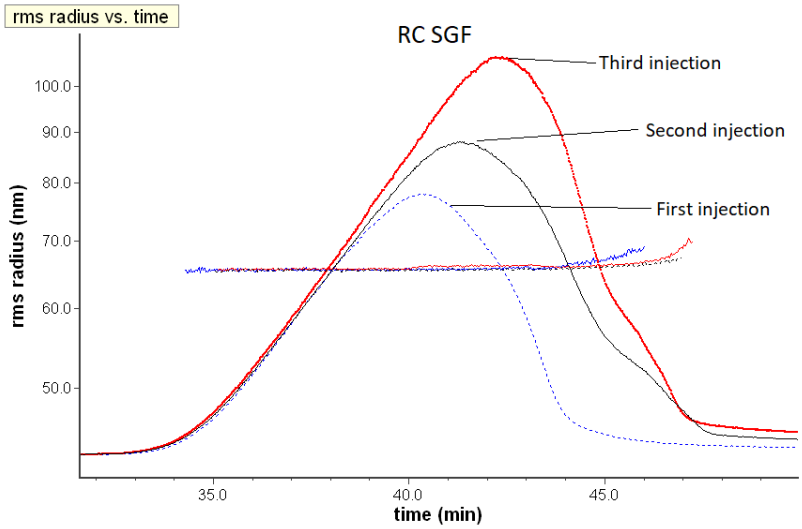

Fig. 8 MALS signal from 3 identically prepared silica samples in SGF conditions, sequentially injected to AF4 with RC membrane and SGF as carrier liquid. The retention time of the peak maximum increases for each injected sample. The r_{rms} are the same for all three peaks. The recovery of particles increases with each injected sample.

The poor recovery suggests interaction with the membrane, to confirm this theory a focus flow is applied to the channel, this will gather particles immobilized to the membrane. The gathered particles are then eluted without any crossflow. The signal obtained from this step Fig. 9, shows peaks after focusing step indicating that silica particles are loosely adsorbed to the membrane and can be washed off.

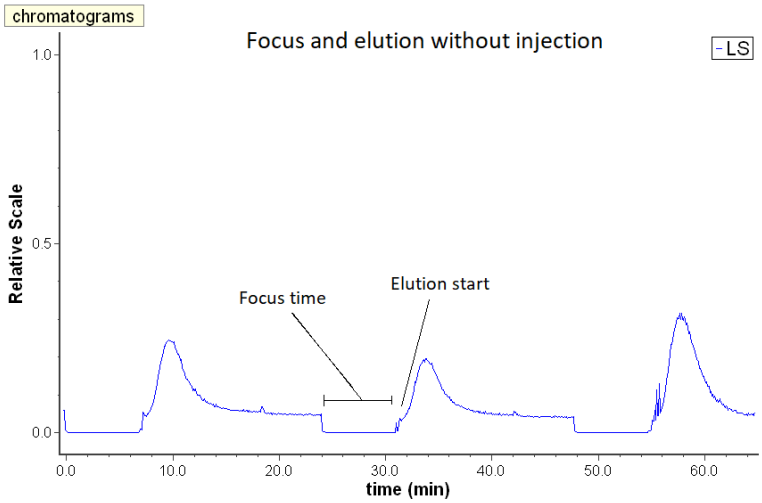

Fig. 9 Focus flow are applied to the membrane to concentrate immobilized particles, then eluted without any crossflow to detect the presence of any particles. The MALS signal shows peak after focus time indicating the presence of particles.

Hypothesis on membrane interaction and peak profile

The diffusion and the cross flow will create a concentration profile close to the membrane, where the concentration is highest closest to the membrane and decrease with the distance from the membrane, the particles closest to the membrane may interact with the membrane retarding its elution, the particles further away from the membrane have no interaction with the membrane. Due

to the laminar flow profile inside the channel the particles away from the membrane is in a higherflow velocity making these particles elute first, these particles did not interact with the membrane and therefore have the same elution time. Most of the particles are close to the membrane due to cross flow and may interact with the membrane changing the retention time, these particles elute at peak maximum. The interaction to RC membrane is weak and particles adsorb and desorb to the membrane.

4.2.3. PES membrane

Silica particles are subjected to the ionic conditions in the intestinal fluid (SIF) in both sample and carrier liquid are SIF. The samples are analyzed using AF4 with PES membrane coupled with MALS and dRI detector (Appendix. 3). The first 5 samples (identically prepared) are presented in Fig. 10. The shape of the peaks is more symmetrical than for RC membrane, the retention time for the peak maximum increases for each injection. The starting point of the peak (time silica particle starts to elute) increases as well, this suggest a change in retention time for all silica particles. Initially the recovery of silica particles increases with each injection, but after the third injection the recovery starts to drop, after 9 injections the recovery of silica particles becomes too low to be detectable by dRI, the results indicate a strong particle adsorption. After preforming the same cleaning step as RC membrane, (applying focus flow to the membrane to gather immobilized particles and then elute without any crossflow) no peaks is recorded i.e. no particles is washed out.

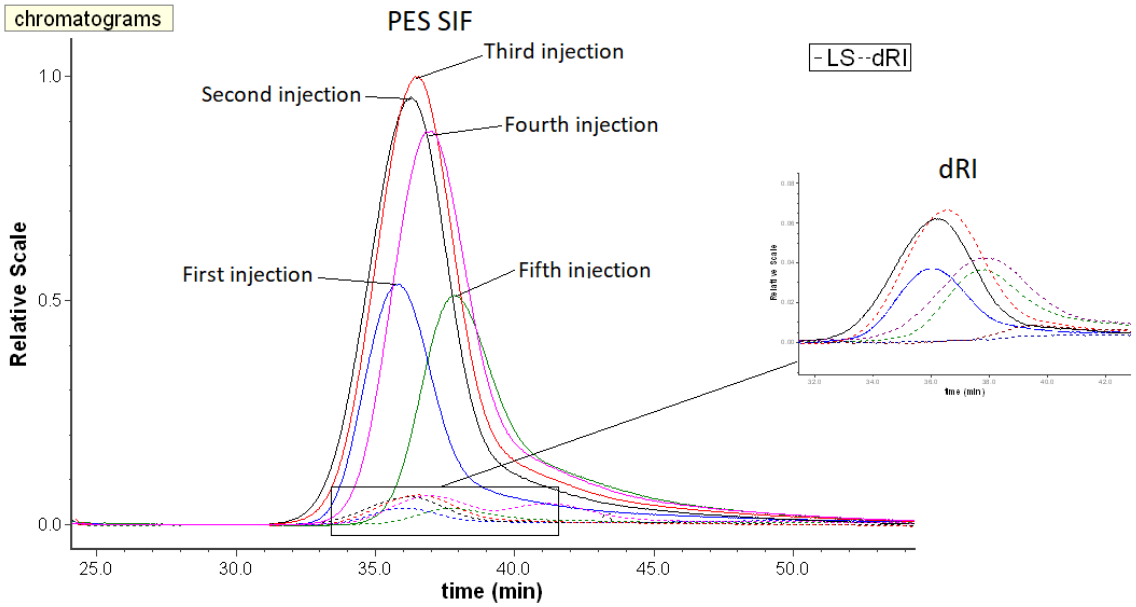

Fig. 10 MALS and dRI signal from 5 identically prepared silica samples in SIF conditions, sequentially injected to AF4 with RC membrane and SIF as carrier liquid. The retention time increases for all particles after each injected sample. The recovery of particles increases for the first three samples and then decreases for the following samples.

Hypothesis on membrane interaction and peak profile

The elution profile of PES showed adsorption kinetics faster than RC-membrane, the adsorption is also stronger, as the contact angle of PES membrane is higher than RC membrane. The initial theory about the shift of the entire peak is due to changes in channel thickness, as particles adsorb to the membrane permanently. If channel thickness changes the retention time of all the particles will be

influenced. However, the shift in retention time increases with each injection. But according to Eq. 3 the retention time should decrease with smaller channel thickness.

4.2.4. PF membrane

Silica particles are subjected to the ionic conditions of SGF in both sample and carrier liquid. PF membrane is used for this trial. The samples are analyzed using AF4 coupled with MALS detector (Appendix. 3). This membrane gave poor recovery and peak-splitting behavior, where particles with the same r_{rms} divide themselves into two peaks Fig. 11. This membrane is not investigated further.

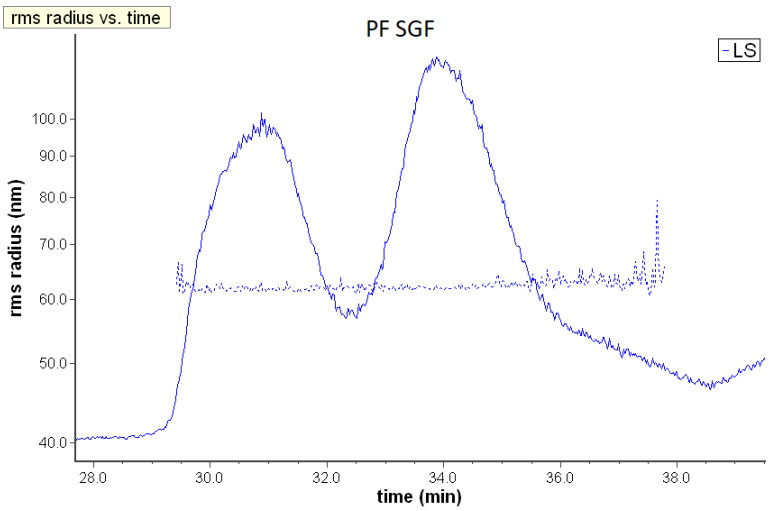

Fig. 11 MALS signal and r_{rms} from silica sample in SGF condition injected to AF4 with PF membrane and SGF as carrier liquid. The recovery is poor and the separation causes a peak splitting behavior where particles with same r_{rms} have different retention times.

4.2.5. Membrane interaction

An AF4 method where the sample conditions and carrier conditions are the same throughout the experiment is unfortunately not possible due to membrane interaction. The information obtained from the calculations and experiments gives an insight about particle-particle, particle-membrane interaction. When the ionic strength increases the Debye length of the particle decreases, short Debye length allows particles to get closer to each other and to the membrane. The closer distance of surfaces leads to greater possibility of attractive interaction. The particle interaction with the membrane can be both sterically and electrostatic. The electrostatic interaction can be calculated, but without reliable values of membrane Z-potential, the electrostatic interaction can only be estimated between particles. The possible physical interaction is due to the fibrous nature of cellulose membrane, it makes it possible for particles to get entangled in the fibers. Contact angle can give additional information about membrane interaction. The less polar PES membrane can lead to adsorption of particles.

4.3. AF4 analysis

The method development concludes that using RC membrane as the accumulation wall and phosphate buffer at pH7 as the carrier liquid is the most suitable setup for this experiment. The silica particles are subjected to the digestive conditions inside the sample vial. The impact of different factors like pH, presence of enzymes and bile salts are considered. The samples are analyzed using AF4 coupled with MALS and dRI detectors. The setup of the system is shown in Appendix.3. Note that all methods use a logarithmic decay cross flow. See Appendix 1.

4.3.1. Gastric condition

The DLVO calculations Fig. 4 indicated that the low pH of the gastric condition does not provide any electrostatic repulsion, therefore particles in SGF_pH should start to aggregate. Fig. 13 shows three identically prepared silica samples subjected to the SGF_pH conditions and analyzed using AF4, the MALS signal shows one main peak for the unaggregated particles at around 34 min with r_{rms}=63nm the second peak at around 37 min shows aggregates with r_{rms} around 100 nm which suggest aggregates of dimer and trimer. At longer retention times the larger aggregates start to elute.

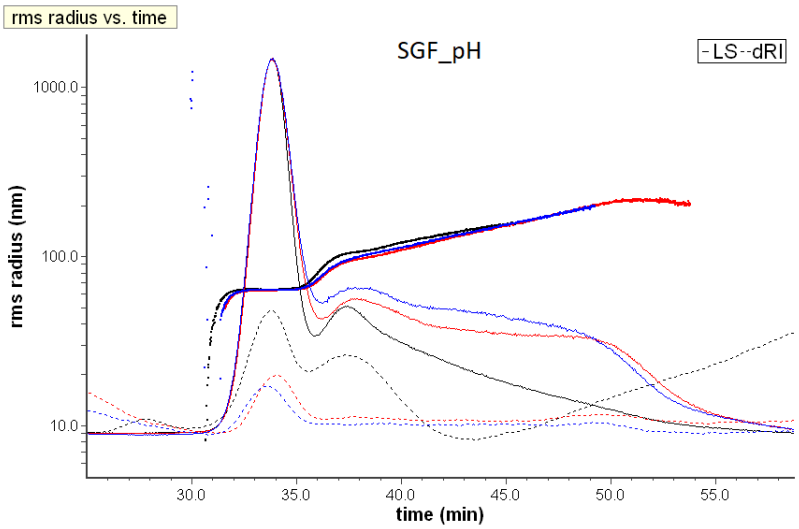

Fig. 12 MALS and dRI signal from 3 identically prepared silica samples in SGF_pH conditions, sequentially injected to AF4 with RC membrane and phosphate buffer pH7 as carrier liquid. The retention time of the main peak of unaggregated particles at 34 min shows a r_{rms} = 63nm and, the following peaks >36 min are of aggregates.

The aggregation is irreversible process therefore reproducibility cannot be obtained. The course of aggregation is investigated by injecting 3 samples with different residence times inside sample vial Fig. 13. The first peak shows the unaggregated particles with r_{rms}=63nm, which makes it possible to compare the concentration of un aggregated particles between different times. The area of first peak shrinks as residence times (inside the sample) increases, suggesting that the amount of aggregates increases with time.

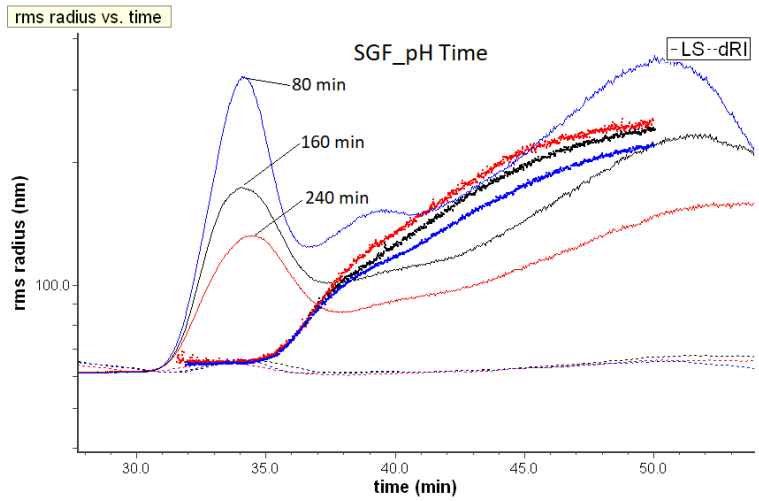

Fig. 13 MALS and dRI signal from the same silica sample with 3 different residence time in SGF_pH conditions, sequentially injected to AF4 with RC membrane and phosphate buffer pH7 as carrier liquid. The retention time of the main peak of un aggregated particles at 34 min shows a r_{rms} = 63nm, the main peak decreases in size as time progresses indicating that unaggregated particles aggregates, the following peaks >36 min are of aggregates.

When particles are subjected to SGF conditions with enzyme present the aggregation occurs like in SGF_pH conditions. Three identically prepared samples are injected to AF4, The MALS signal shows a main peak (at 34 min) with unaggregated particles and the aggregates at retention time >37min Fig 14. From calculation see Table.6 the enzymes will cover 0.06mg/m2, this is insufficient to cover the surface with proteins, concentration of 1-5 mg/m2 is required. Since most the surface of the particles is uncovered the enzymes cannot contribute steric repulsion to the particles, and a possible reason for aggregation is bridging.

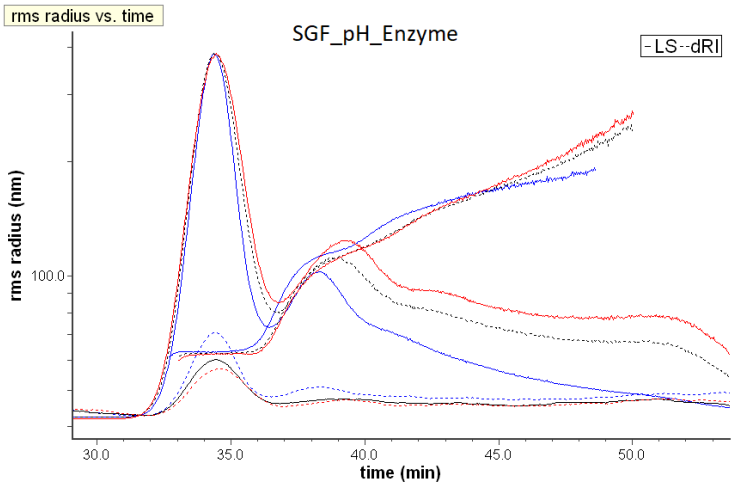

Fig. 14 MALS and dRI signal from 3 identically prepared silica samples in SGF_pH_Enzyme conditions, sequentially injected to AF4 with RC membrane and phosphate buffer pH7 as carrier liquid. The chromatogram shows similar aggregation behavior as SGF_pH, the retention time of the main peak of unaggregated particles at 34 min shows a r_{rms} = 63nm and, the following peaks >36 min are of aggregates.

The aggregation does not reach any equilibrium. The course of aggregation is investigated by injecting 3 samples with different residence times inside the sample vial Fig. 15. The first peak shows the unaggregated particles with r_{rms}=63nm, the area of this peak shrinks as residence times

increases, suggesting that the amount of unaggregated particles reduces with time. Following peaks (Retention time >37) min arrives from aggregates,

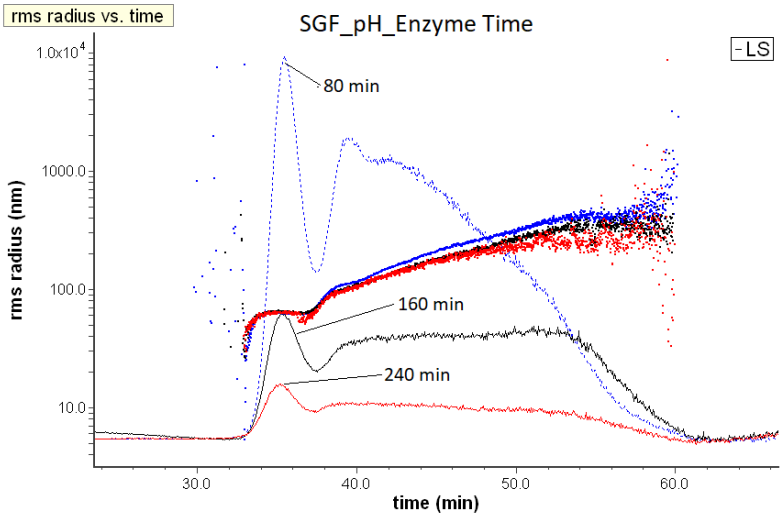

Fig. 15 MALS and dRI signal from the same silica sample with 3 different residence time in SGF_pH_Enzyme conditions, sequentially injected to AF4 with RC membrane and phosphate buffer pH7 as carrier liquid. The retention time of the main peak of unaggregated particles at 34 min shows a r_{rms} = 63nm, the main peak decreases in size as time progresses indicating that unaggregated particles aggregate, the following peaks >36 min are of aggregates.

4.3.2. Intestinal condition

The DLVO calculations Fig. 4 indicates that conditions in SIF_pH provides more colloidal stability than in SGF_pH. Fig. 16 shows three identically prepared samples subjected to SIF_pH conditions analysed with AF4, the MALS signal shows one main peak for the unaggregated particles at around 34 min with $\mathrm{r_{rms}}$=63nm and a second small peak at around 37 min where aggregates have $\mathrm{r_{rms}}$ around 100 nm, close to double the size of single particle which suggest aggregates of dimer and trimer, no significant amount of larger aggregates can be observed suggesting SIF_pH conditions are more stable than SGF_pH.

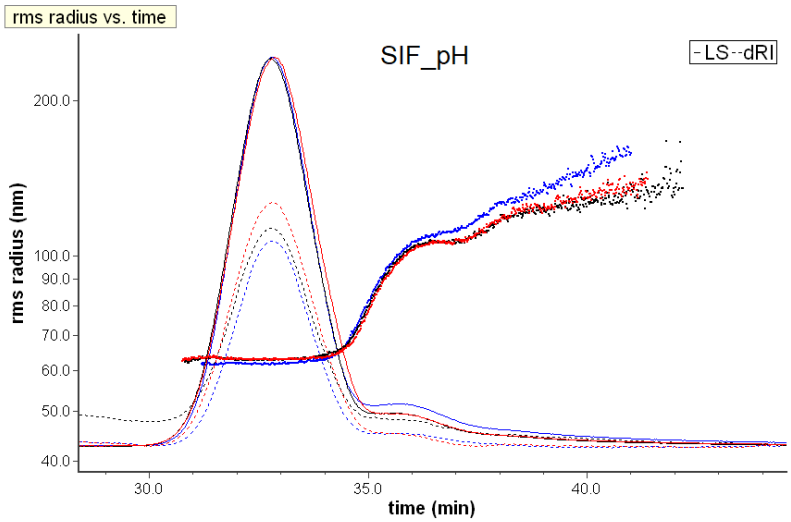

Fig. 16 MALS and dRI signal from 3 identically prepared silica samples in SIF_pH conditions, injected to AF4 with RC membrane and phosphate buffer pH7 as carrier liquid. The retention time of the main peak of unaggregated particles at 34 min shows a r_{rms} = 63nm and, the following peaks >36 min are of aggregates. The aggregation is not as rapid as in SGF_pH conditions due to higher electrostatic repulsion.

Unlike the particles in SGF_pH the particles SIF_pH has some electrostatic repulsion, which leads to a slower aggregation. The course of aggregation is investigated by injecting 3 samples with different residence times inside the sample vial Fig. 17. The dRI suggest a decrease of unaggregated particles but no bigger aggregates are formed rapidly (no large peaks at >37min), witch suggest a slow aggregation behavior.

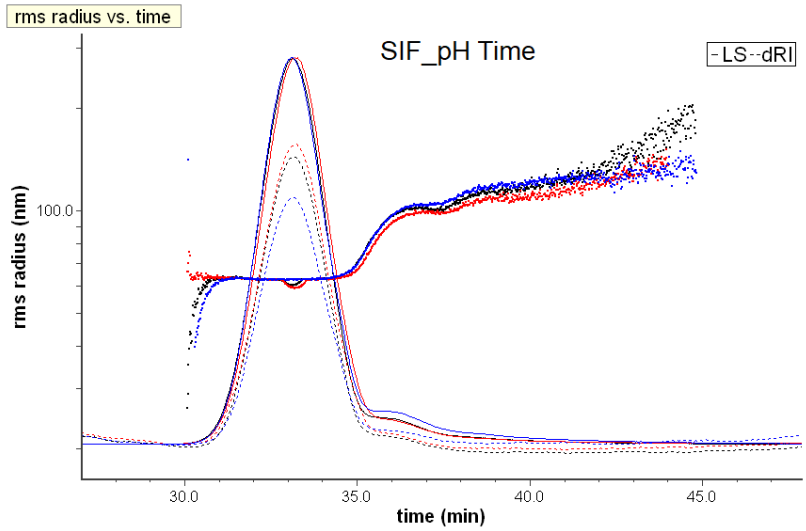

Fig. 17 MALS and dRI signal from the same silica sample with 3 different residence time in SIF_pH_Enzyme conditions, sequentially injected to AF4 with RC membrane and phosphate buffer pH7 as carrier liquid. The retention time of the main peak of unaggregated particles at 34 min shows a r_{rms} = 63nm, the aggregation rate is slow, the following peaks >36 min are of aggregates.

When the particles are subjected to SIF conditions with enzymes added the aggregation kinetics changes drastically. The MALS signal Fig. 18 shows how components with larger $\mathrm{r_{rms}}$(>100nm) are eluted in the beginning of elution, the decreasing size with time is due to coelution of small un aggregated particles (Brownian mode) and large aggregated particles (Steric-Hyperlayer mode) the

size obtained from MALS is a average of these co eluted particles. The main peak (at 34 min) have a peak maximum with r_{rms}=63nm, the peak consists of both unaggregated and aggregated particles. The aggregation happens rapidly as big aggregates form in a short period of time. From calculation see Table.6 the high enzyme concentration in SIF ensures total coverage of the particle surface. Since the surface is covered the most probable reason for aggregation is protein-protein interaction.

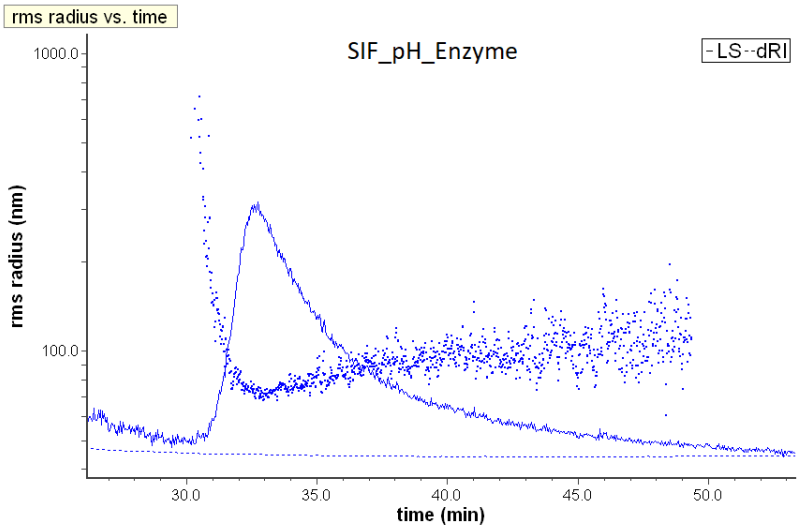

Fig. 18 MALS and dRI signal of silica sample in SIF_pH_Enzyme conditions, injected to AF4 with RC membrane and phosphate buffer pH7 as carrier liquid. Particles with larger r_{rms} are eluted in the beginning of elution, it is possible that these consist of aggregated proteins. The main peak consists of both unaggregated and aggregated particles, the unaggregated particle elute at 34 min with a r_{rms}=63 nm followed by aggregates. The aggregation rate is fast as large aggregates form in a short period of time.

When silica particles are moved of SGF_pH_Enzyme to SIF_pH_Enzyme Fig. 19, similar results are obtained where larger components elute in the beginning of elution, followed by a peak with unaggregated particles and aggregates. The aggregation rate in SGF_pH_Enzyme Fig.14 is slower compared with SIF_pH_Enzyme Fig. 18 which concludes that most of the aggregation happens under SIF_pH_Enzyme conditions.

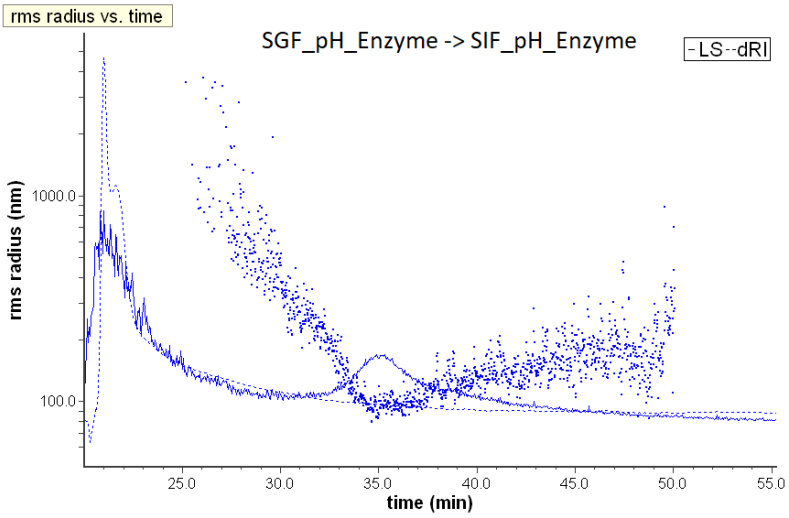

Fig. 19 MALS and dRI signal of silica sample in SIF_pH_Enzyme conditions, injected to AF4 with RC membrane and phosphate buffer pH7 as carrier liquid. The peak at 35 min consists of both unaggregated and aggregated

particles. It is possible that the bigger particles eluted in the beginning of elution consist of aggregated proteins, the aggregation rate is fast as large aggregates form in a short period of time.

4.3.3. Bile salt

The last parameter to look at is the effect of bile salt. Bile is mixed with both the gastric and intestinal conditions with all enzymes present. Bile salt acts as a surfactant adsorbing to surfaces and contribute to the electrostatic repulsion. The concentration of bile far exceeds the concentration of enzymes in both SGF and SIF conditions. Due to the dominant numbers of bile salt the flux to the particle surface will be dominated by the bile salt. In the gastric conditions where the aggregation occurs due to lack of electrostatic repulsion and bridging Fig. 14 the bile salt will cover the surface and contribute to electrostatic repulsion preventing rapid aggregation. Bile salt is added to SGF_pH_Enzyme and analyzed with AF4. the main peak at 34 min shows the unaggregated particles and only a small amount small aggregates >40 min Fig 20. The first peak from dRI shows the high concentration of bile salt and its aggregates. Compared with SGF_pH_Enzyme conditions in Fig.14 the aggregation is slower indicating added electrostatic stabilization provided by bile salt.

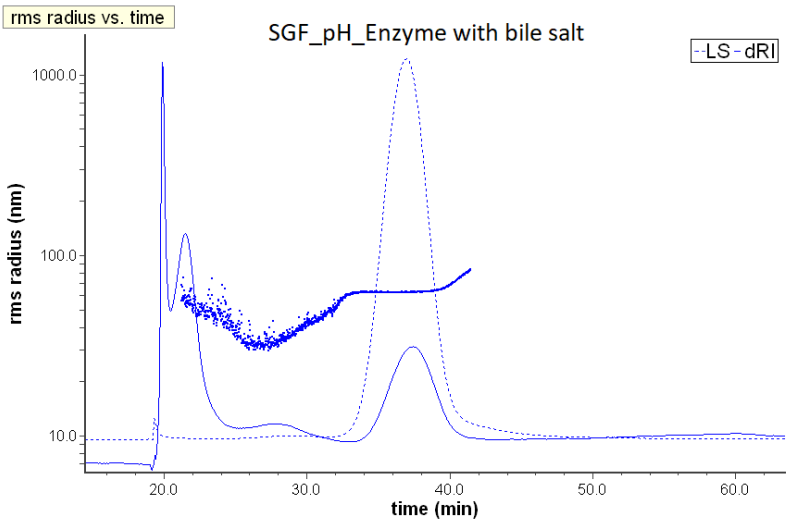

Fig. 20 MALS and dRI signal of silica sample in SGF_pH_Enzyme conditions with bile salt added, injected to AF4 with RC membrane and phosphate buffer pH7 as carrier liquid. The first peak from dRI shows the high concentration of bile salt and its aggregates. The peak at 35 min consists of the unaggregated particles. There are no signs of larger aggregates and indicates a slow aggregation. Compared with SGF_pH_Enzyme conditions Fig.14 the aggregation is slower indicating added electrostatic stabilization provided by bile salt.

In the SIF the conditions are very different, the vast numbers of proteins of different kind makes is difficult to evaluate the event. Fig.21 shows the MALS signal from sample with silica particles introduced to SIF_pH_Enzyme with Bile salt, the sample is analyzed 18h after preparation. The peak start at 35 min and ends at 60 min where the crossflow stops. Even if this gives a wide range of r_{hyd} (wide range of retention time) the r_{rms} keeps relatively constant throughout the peak. The conformation of the adsorbed layer is hard to estimate, possible conformations are; monolayer of bile salt, a mix of different proteins and bile salt, or different layers of bile salt and protein sandwiched between each other creating several layers. Compare the results from Fig 18 the aggregation is less rapid witch indicates that bile salt prevents some aggregation. The reason no big aggregates where detected could be sedimentation inside the vial and thus not injected into the channel.

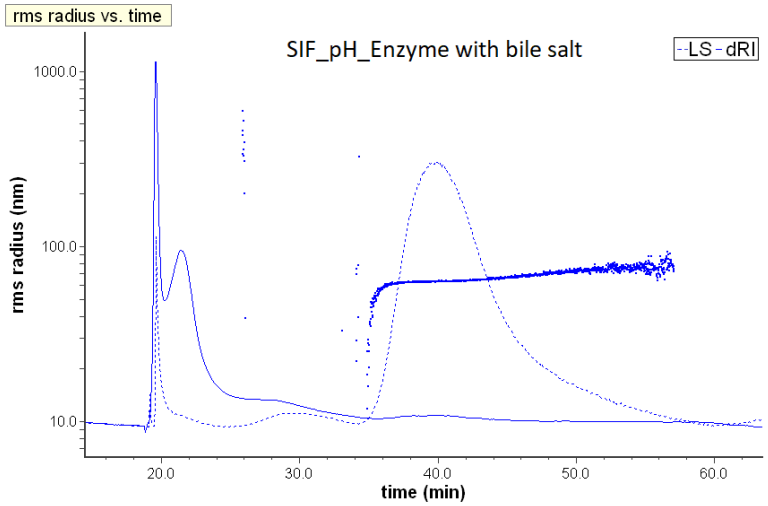

Fig. 21 MALS and dRI signal of silica sample in SIF_pH_Enzyme conditions with bile salt added, The sample is injected to AF4 after a residence time of 18 hours in the sample vial. The first peak from dRI shows the high concentration of bile salt and its aggregates. The peak at 40 min consists of the unaggregated particles with r_{rms}=64nm and keeps close to constant throughout the elution, there are no signs of larger aggregates. Compared with Fig.18 the aggregation process has stalled, indicating added stabilization provided by bile salt. The reason no big aggregates where detected could be sedimentation inside the vial and thus not injected into the channel.

5. Conclusion

5.1. Conclusion method development

To avoid membrane interaction and not influence the aggregation the membrane with the highest surface energy which is the Regenerated cellulose membrane are most suitable, the choice of carrier liquid will influence both particle-membrane interaction and particle-particle interaction. as neither interactions are desirable in the channel a suitable carrier should provide a strong electrostatic repulsion, therefore the solution should be a low ionic strength buffer with a pH away from the isoelectric point of the particle. This will prevent further aggregation in the channel and keep the particles/aggregates away from membrane.

5.2. Conclusion experiments.

The main goal of this project is to estimate the aggregation behavior of nanoparticles under gastro intestinal conditions. To see if nanoparticles are kept dispersed and therefore cause damage. Aggregation occurs both by the lack of electrostatic repulsion in the low pH environment of SGF and by protein interaction, bridging and protein-protein interaction. Bile salt acts as a surfactant encapsulating particles and proteins. The contribution to the stability is most likely by electrostatic repulsion. The stability provided by bile salt makes it possible for Nano silica to be freely suspended in the intestinal tract and therefore a possibility to cause damage by penetrating the intestinal membrane. Even if this study only looks at very few parameters in an otherwise very complex system that is food and digestive system, the conclusion remains that it is possible to have feely dispersed Nano silica in the digestive system when it is consumed in food.

6. Future work

The main goal of the project is to investigate the aggregation behavior of silica inside the digestive system, this work only investigated a small part of this complex issue. Factors like food components and the variation in the digestive system is not concerned. The mechanisms on how bile salt contributes to stabilization is still unclear and needs to be investigated further. For future work factors like lipids carbohydrates and proteins should also be incorporated in the experiment.

The particle-membrane interaction is still not understood, further investigation on the membrane with SEM microscope on both covered and uncovered membrane will give additional insight on interaction behavior. Surface Z-potential measurement can be optimized to give accurate potential, both covered and uncovered membranes is measured to give information on the change in electrostatic interaction.

Appendix 1

Table 1. Normalization using BSA

Mode	Duration	Cross flow start (mL/min)	Cross flow end (mL/min)
Elution	1 min	3.00	3.00
Focus	1 min		
Focus + injection	2 min		
Focus	3 min		
Elution	25 min	0.30	0.30
Elution + injection	5 min	0	0
Flow settings			
Carrier liquid	50mM NaNO3		
Focus flow	3.00 ml / min		
Injection flow	0.20 ml / min		
Detector flow	1.00 ml / min		

Table 2. RC MQ

Mode	Duration	Cross flow start (mL/min)	Cross flow end (mL/min)
Elution	1 min	0	0
Focus + injection	4 min		
Focus	5 min		
Elution	43 min	0.2	0.2
Elution + injection	7 min	0	0
Flow settings			
Carrier liquid	MQ water		
Focus flow	1ml / min		
Injection flow	0.2 ml / min		
Detector flow	1 ml / min		

Table RC SGF

Mode	Duration (min)	Cross flow start (mL/min)	Cross flow end (mL/min)
Elution	1 min	0.3	0.3
Focus + injection	5 min		
Focus	5 min		
Elution	120 min	0.3	0.3
Elution + injection	7 min	0	0
Flow settings			
Carrier liquid	SGF		
Focus flow	0.3 ml / min		
Injection flow	0.2 ml / min		
Detector flow	1.1 ml / min		

PES SGF

Mode	Duration	Cross flow start (mL/min)	Cross flow end (mL/min)
Elution	2 min	0.3	0.3
Focus	1 min		
Focus + injection	10 min		

Focus	10 min		
Elution	30 min	0.2	0.2
Elution	20 min	0.2	0.02
Elution + injection	10 min	0	0
Flow settings			
Carrier liquid	SGF		
Focus flow	0.2ml / min		
Injection flow	0.2 ml / min		
Detector flow	1 ml / min		

PES SIF

Mode	Duration	Cross flow start (mL/min)	Cross flow end (mL/min)
Elution	2 min	0.3	0.3
Focus	1 min		
Focus + injection	10 min		
Focus	10 min		
Elution	30 min	0.2	0.2
Elution	20 min	0.2	0.02
Elution + injection	10 min	0	0
Flow settings			
Carrier liquid	SIF		
Focus flow	0.2ml / min		
Injection flow	0.2 ml / min		
Detector flow	1 ml / min		

PF MQ

Mode	Duration	Cross flow start (mL/min)	Cross flow end (mL/min)
Elution	1 min	0.3	0.3
Focus + injection	4 min		
Focus	10 min		
Elution	43 min	0.3	0.3
Elution + injection	7 min	0	0
Flow settings			
Carrier liquid	MQ water		
Focus flow	0.3 ml / min		
Injection flow	0.2 ml / min		
Detector flow	1 ml / min		

RC phosphate ph3 SGF_pH_enzyme

Mode	Duration	Cross flow start (mL/min)	Cross flow end (mL/min)
Elution	1 min	0.50	0.50
Focus	1 min		
Focus + injection	10 min		
Focus	7 min		
Elution	4 min	0.50	0.36
Elution	4 min	0.36	0.28
Elution	4 min	0.28	0.23

Elution	4 min	0.23	0.20
Elution	4 min	0.20	0.18
Elution	4 min	0.18	0.17
Elution	4 min	0.17	0.16
Elution	4 min	0.16	0.16
Elution	4 min	0.16	0.15
Elution	4 min	0.15	0.15
Elution	4 min	0.15	0
Elution + injection	5 min	0	0

Flow settings	
Carrier liquid	Phosphate pH3
Focus flow	0.50 ml / min
Injection flow	0.20 ml / min
Detector flow	1.00 ml / min

RC phosphate pH7 SGF_pH

Mode	Duration	Cross flow start (mL/min)	Cross flow end (mL/min)
Elution	1 min	0.50	0.50
Focus	1 min		
Focus + injection	10 min		
Focus	7 min		
Elution	4 min	0.50	0.36
Elution	4 min	0.36	0.28
Elution	4 min	0.28	0.23
Elution	4 min	0.23	0.20
Elution	4 min	0.20	0.18
Elution	4 min	0.18	0.17
Elution	4 min	0.17	0.16
Elution	4 min	0.16	0.16
Elution	4 min	0.16	0.15
Elution	4 min	0.15	0.15
Elution	4 min	0.15	0
Elution + injection	5 min	0	0

Flow settings	
Carrier liquid	Phosphate pH7
Focus flow	0.50 ml / min
Injection flow	0.20 ml / min
Detector flow	1.00 ml / min

RC phosphate pH7 SGF_pH_Enzyme

Mode	Duration	Cross flow start (mL/min)	Cross flow end (mL/min)
Elution	1 min	0.50	0.50
Focus	1 min		
Focus + injection	10 min		
Focus	7 min		
Elution	4 min	0.50	0.36
Elution	4 min	0.36	0.28
Elution	4 min	0.28	0.23
Elution	4 min	0.23	0.20

Elution	4 min	0.20	0.18
Elution	4 min	0.18	0.17
Elution	4 min	0.17	0.16
Elution	4 min	0.16	0.16
Elution	4 min	0.16	0.15
Elution	4 min	0.15	0.15
Elution	4 min	0.15	0
Elution + injection	5 min	0	0

Flow settings	
Carrier liquid	Phosphate pH7
Focus flow	0.50 ml / min
Injection flow	0.20 ml / min
Detector flow	1.00 ml / min

RC phosphate pH7 SIF_pH

Mode	Duration	Cross flow start (mL/min)	Cross flow end (mL/min)
Elution	1 min	0.50	0.50
Focus	1 min		
Focus + injection	10 min		
Focus	7 min		
Elution	4 min	0.50	0.36
Elution	4 min	0.36	0.28
Elution	4 min	0.28	0.23
Elution	4 min	0.23	0.20
Elution	4 min	0.20	0.18
Elution	4 min	0.18	0.17
Elution	4 min	0.17	0.16
Elution	4 min	0.16	0.16
Elution	4 min	0.16	0.15
Elution	4 min	0.15	0.15
Elution	4 min	0.15	0
Elution + injection	5 min	0	0

Flow settings	
Carrier liquid	Phosphate pH7
Focus flow	0.50 ml / min
Injection flow	0.20 ml / min
Detector flow	1.00 ml / min

RC phosphate pH7 SIF_pH_Enzyme

Mode	Duration	Cross flow start (mL/min)	Cross flow end (mL/min)
Elution	1 min	0.50	0.50
Focus	1 min		
Focus + injection	10 min		
Focus	7 min		
Elution	4 min	0.50	0.36
Elution	4 min	0.36	0.28
Elution	4 min	0.28	0.23

Elution	4 min	0.23	0.20
Elution	4 min	0.20	0.18
Elution	4 min	0.18	0.17
Elution	4 min	0.17	0.16
Elution	4 min	0.16	0.16
Elution	4 min	0.16	0.15
Elution	4 min	0.15	0.15
Elution	4 min	0.15	0
Elution + injection	5 min	0	0

Flow settings	
Carrier liquid	Phosphate pH7
Focus flow	0.50 ml / min
Injection flow	0.20 ml / min
Detector flow	1.00 ml / min

Appendix.2 Infogest in vitro digestion and phosphate buffer*.

Constituent	Stock conc. g/L	Stock conc. mol/L	Conc. In SGF (mol/L)	Vol of stock added (ml)	Conc. In SIF mol/L	Vol of stock added (ml)
KCL	37.3	0.5	0.0069	13.8	0.0068	13.6
KH2PO4	68	0.5	0.0009	1.8	0.0008	1.6
NaHCO3	84	1	0.025	25	0.085	85
NaCl	117	2	0.0472	23.6	00384	19.2
MgCl2(H2O)6**	30.5*	0.15	0.0001	0.666666	0.00033	2.2
(NH4)2CO3	48	0.5	0.0005	1		0
CaCl2(H2O)2	44.1	0.3	0.00075	2.5	0.003	10
			pH3		pH7	
NaOH	40	1	/	/	/	/
HCl	219	6	0.0156	2.6	0.0084	1.4

Porcine pepsin	2U/mL			
Pancreatin				
Bile salt			10mM	
Phospholipids	0.17mM			

	Phosphate buffer pH7		Phosphate buffer pH 3	
	mM	g/L	mM	g/l
Na_2HPO_4	5.77	0.952	0	0
NaH_2PO_4	4.23	0.592	10	1.4

*MgCl2 are used instead (95.2g/mol) stock conc =14.28g/L

**All liquids contain 3mM NaN3.

Appendix. 3

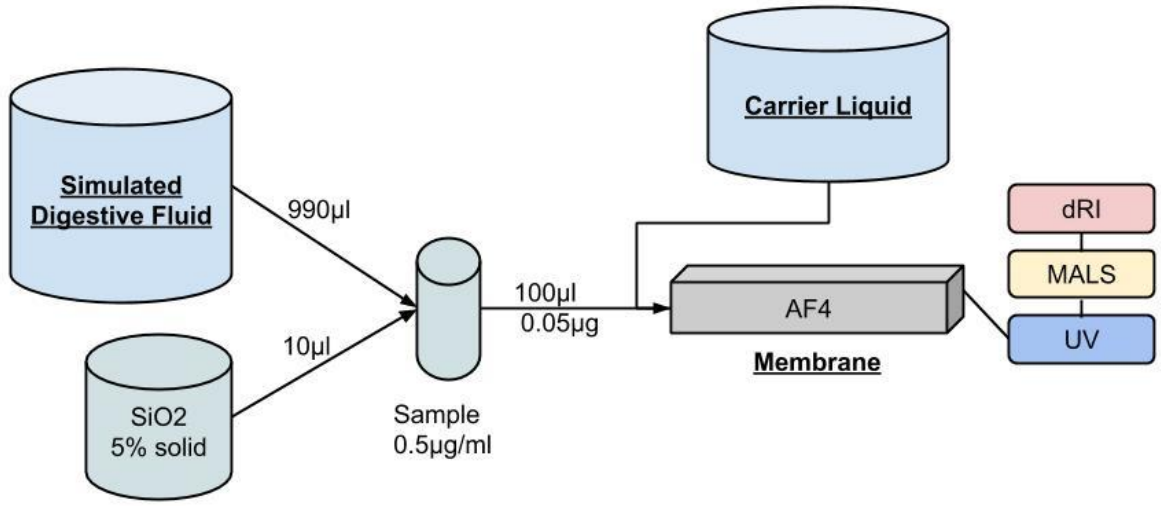

Trial 1

Simulated Digestive Fluid	Carrier Liquid	Membrane
MQ	MQ	Regenerated Cellulose
SGF	SGF	

Trial 2

Simulated Digestive Fluid	Carrier Liquid	Membrane
SGF	SGF	Poly Ether Sulfone
SIF	SIF	

Trial 3

Simulated Digestive Fluid	Carrier Liquid	Membrane
SGF	SGF	Poly-Fluorinated

Trial 4

Simulated Digestive Fluid	Carrier Liquid	Membrane
SGF_pH	Phosphate pH3	Regenerated Cellulose
SGF_pH	Phosphate pH7	
SGF_pH_Enzyme		
SIF_pH		
SIF_pH_Enzyme		
SGF_pH_Enzyme		
SIF_pH_Enzyme		

Appendix. 4 Calculations

Sample parameters

Total sample volume	1 ml
Colloidal silica amount in sample	10ul
Amount silica in sample	0.0005g= 0.5mg
Amount silica injected (100µl)	50 µl
Molar mass based on dRI (5 samples)	1.39*10^9 g/mol
Density SiO_2	$2.65 g/ml$

Surface area for spherical particles with 150nm diameter.

$$A = 4\pi r^2 = 4 * 3.14 * 75^2 = 70685 nm^2/partikel\ (7.0685 * 10^{-14} m^2)$$

Volume for spherical particles with 150nm diameter.

$$V = \frac{4}{3}\pi r^3 = \frac{4}{3} * 3.14 * 75^3 = 17671{,}5 nm^3/particle\ \ (1.76715 * 10^{-23} m^3)$$

Amount particles in sample based on dRI.

$$\frac{m}{M} = n = \frac{0{,}0005\ g}{1.39 * 10^9\ g/mol} = 3.6 * 10^{-13}\ mol$$

$$n * N_A = 3.6 * 10^{-13} mol * 6.022 * 10^{23} = 2.166 * 10^{11}\ particles$$

Surface area of SiO_2 in sample based on dRI

$$A * n = 7.0685 * 10^{-14} m^2 * 2.166 * 10^{11} = 0.0153\ m^2$$

Enzyme parameters

	SGF	SIF
Required enzyme activity	2000u/L pepsin	100000u/ml Pancreatin (trypsin activity)
Activity of enzyme	2240u/mg	100usp/mg (trypsin activity)
Amount enzyme in solvent	0.89 mg/l	1000mg/l
Amount enzyme in sample	0.00089 mg	1 mg

Enzyme coverage of silica in sample vial

$$SGF_{Enzyme\ coverage} = \frac{Amount\ of\ Enzyme}{Area} = \frac{0{,}00089 mg}{0{,}0153 m^2} = 0.0581 mg/m^2$$

$$SIF_{Enzyme\ coverage} = \frac{Amount\ of\ Enzyme}{Area} = \frac{1 mg}{0.0153 m^2} = \frac{65.3 mg}{m^2}$$

dn/dc

$(0.2\mu m - 200\mu m)\ n_{H_2O} = 1.3325$ dRI wavelenght 690nm

$$v = \frac{dn}{dc} => \lim_{c_0 \to 0} \left(\frac{n - n_0}{c - c_0}\right)$$

$$v_{SiO_2 in\ H_2O} = 0.0833$$

Appendix.5 Coverage of PES-Membrane

Surface area Membrane

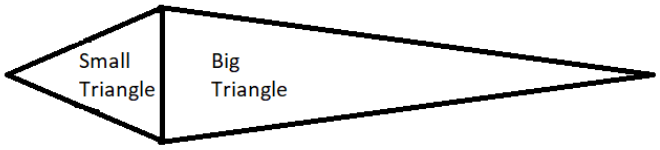

$$\text{Small triangle} + \text{Big triangle} = \frac{0.024 * 0.02}{2} + \frac{(0.179 - 0.02) * 0.024}{2} = 0.00218\text{m}^2$$
$$= 21.8\text{cm}^2 \ (19\text{cm}^2 \text{ area after inlet})$$

Surface coverage by Silica

$$150\text{nm} * 150\text{nm} = 2.25 * 10^{-10}\text{cm}^2/\text{particle}$$

1 injection of 50ug silica have 2.166*10^11 particles and covers 48.7 cm2

$$\frac{19\text{cm}^2}{2.25 * 10^{-10}\text{cm}^2/\text{particle}} = 8.44 * 10^{10}\text{particles (to cover surface with monolayer)}$$

Silica particles

Sample	Injected amount (ug)	Recovered amount (ug)	Adsorbed membrane (ug)	% adsorbed / interacted	Covered area	Number of monolayers	thickness of layer (um)
1	50	20	30	60	29.4	1.547368421	0.232105263
2	50	25	25	50	24.5	1.289473684	0.193421053
3	50	32	18	36	17.64	0.928421053	0.139263158
4	50	43.66	6.44	12.88	6.311	0.332157895	0.049823684
5	50	29.2	20.8	41.6	20.38	1.072631579	0.160894737
seq 1	50	35.57	14.43	28.86	14.14	0.744210526	0.111631579
seq 2	50	17.07	32.93	65.86	32.27	1.698421053	0.254763158
seq 3	50	12.08	27.92	55.84	27.36	1.44	0.216
seq 4	50	6.3	43.7	87.4	42.82	2.253684211	0.338052632
seq 5	50	2.9	47.1	94.2	46.158	2.429368421	0.364405263
			Sum: 266.32			Sum: 13.73573684	Sum: 2.06

Appendix. 6 Surface Z-potential of membrane

Membrane	Soulution	pH	Ionic strength (mM)	Surface Z-potential	Uncertainty
RC	MQ	10	3	-12.8	3.93
	Phosphate buffer	7	10	2.93	4.43
	Phosphate buffer	3	10	-19.2	4.02
	SGF	8.8	82	-9.51	2.91
	SIF	8.7	132	33.8	7.58
PES	MQ	10	3	-14.4	3.03
	Phosphate buffer	7	10	-20.6	3.92
	Phosphate buffer	3	10	-34.2	5.02
	SGF	8.8	82	-15.2	3.24
	SIF	8.7	132	24.7	14.3
PF	MQ	10	3	12.2	1.86
	Phosphate buffer	7	10	0.653	2.42
	Phosphate buffer	3	10	-15.3	5.96

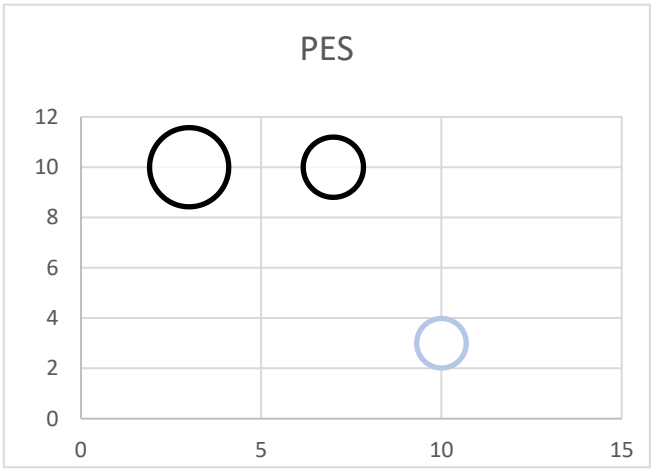

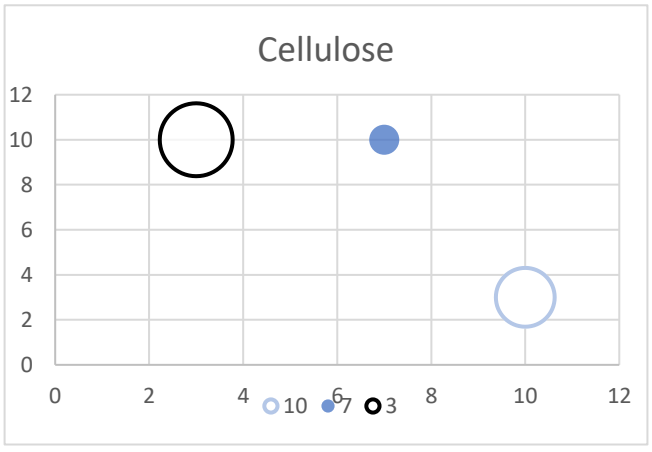

Appendix. 7 Carrier and sample conditions

MQ

Ionic Strength	3.1 mM
Debye length	5.5 nm
pH	10
Z-potential	-30.6 mV

Phosphate buffer pH7

Ionic Strength	19 mM
Debye length	2.66 nm
pH	7
Z-potential	-33.6 mV

Phosphate buffer pH3

Ionic Strength	8 mM
Debye length	3.4 nm
pH	3
Z-potential	3.9 mV

SGF

Ionic Strength	81 mM
Debye length	1.07 nm
pH	8.8
Z-potential	-28.4

SGF_pH

Ionic Strength	81 mM
Debye length	1.07 nm
pH	2.8
Z-potential	2.19 mV

SIF

Ionic Strength	132 mM
Debye length	0.84 nm
pH	8.7
Z-potential	-27.2

SIF_pH

Ionic Strength	132 mM
Debye length	0.84 nm
pH	8.5
Z-potential	23.1

7. References

1. Ruud Peters, E.K., Agnes G. Oomen, Zahira E. Herrera Rivera,† Gerlof Oegema,† Peter C. Tromp,§ Remco Fokkink,^ Anton Rietveld,‡ Hans J. P. Marvin,† Stefan Weigel,† Ad A. C. M. Peijnenburg,† and Hans Bouwmeester†,*, *Presence of Nano-Sized Silica during In Vitro Digestion of Foods Containing Silica as a Food Additive.* American Chemical Society Nano, 2012. **6**: p. 2441–2451.
2. Litzén, A.W., K., *Influence of crossflow hydrodynamics on retention ratio in flow field-flow fractionation.* Analytica Chimica Acta, 1991. **246**(1): p. 161-169.
3. Wahlund, K.-G. and L. Nilsson, *Flow FFF – Basics and Key Applications*, in *Field-Flow Fractionation in Biopolymer Analysis*, S.K.R. Williams and K.D. Caldwell, Editors. 2012, Springer Vienna: Vienna. p. 1-21.
4. Andersson, M., *Asymmetrical Flow Field-Flow Fractionation and Multiangle Light Scattering for Molar mass Analysis of Polysaccharide Derivatives.* 2003.
5. Zielke, C.K., *On the Aggregation of Cereal Beta-Glucan and it's Association with other Biomelecules*, in *Faculty of engineering*. 2017, Lund university: Lund.
6. Nilsson, L., *Separation and characterization of food macromolecules using field-flow fractionation: A review.* Food Hydrocolloids, 2013. **30**(1): p. 1-11.
7. Dickinson, E., *An Introduction to Food Colloids*. 1992, New York Oxford University Press. 207.
8. Arfvidsson, C. and K.-G. Wahlund, *Mass overloading in the flow field-flow fractionation channel studied by the behaviour of the ultra-large wheat protein glutenin.* Journal of Chromatography A, 2003. **1011**(1): p. 99-109.
9. Held, D. *How to Determine dn/dc Values*. 2015. **10**.
10. Polyanskiy, M., *Refractiveindex database*.
11. Håkansson, A., et al., *Hydrodynamic radius determination with asymmetrical flow field-flow fractionation using decaying cross-flows. Part I. A theoretical approach*. Vol. 1253. 2012. 120-6.
12. Malvern, *Zetasizer Nano*

User Manual. 2013, Malvern instruments: UK.

13. Martindale, *Buffer solutions*, in *European pharmacopoeia 5.0*. 2005. p. 430-435.
14. Jiwei Cui, Y.J., Kang Liang, Hirotaka Ejima, Samuel Lörcher, Katelyn T.Gause, Joseph J.Richardson, Frank Caruso, *Nanoscale engineering of low-fouling surfaces through polydopamine immobilization of zwetterionic peptides.* Soft matter, 2014. **10**: p. 2256-2663.
15. Bergström, L., *Hammaker constant of inorganic meterials.* Advances in colloid and interface science, 1997. **70**: p. 125-169.
16. Maryott;, C.G.M.A.A., *Dielectric Constant of water from 0-100.* Journal of Research of the National Bureau of Standards, 1956. **56**.